

ELECTROMAGNETIC MODELING OF INDUCTION TOOL RESPONSES IN
ISOTROPIC AND ANISOTROPIC LAYERED EARTH FORMATIONS

by

Nawayandra Shakya

Submitted in Partial Fulfillment of the Requirements

for the Degree of

Master of Science

in the

Electrical Engineering

Program

YOUNGSTOWN STATE UNIVERSITY

August, 2015

Electromagnetic Modeling of Induction Tool Responses in Isotropic and Anisotropic Layered Earth Formation

Nawayandra Shakya

I hereby release this thesis to the public. I understand that this thesis will be made available from the OhioLINK ETD Center and the Maag Library Circulation Desk for public access. I also authorize the University or other individuals to make copies of this thesis as needed for scholarly research.

Signature:

Nawayandra Shakya, Student Date

Approvals:

Dr. Lin Sun, Thesis Advisor Date

Dr. Philip C. Munro, Committee Member Date

Dr. Salvatore R. Pansino, Committee Member Date

Dr. Salvatore A. Sanders, Dean Graduate Studies and Research Date

ABSTRACT

The study presents the 3D electromagnetic model of layered isotropic and anisotropic media using an induction logging tool. This tool utilizes the electromagnetic wave frequency domain (EWFD) interface with Maxwell's equations. The study shows the effect of conductivity and depth for determining the electric field among single and multiple-layered formations. An induction logging tool operates deep inside the earth surface to measure earth formations and yields real-time formation parameters related to the layer of the earth as a function of depth. COMSOL Multiphysics software designs the induction logging tool, complex voltages are obtained from the 3D COMSOL model for the different layered formation, and MATLAB calculates attenuation and phase shifts. The induction tool is applied to both normal and horizontal directions in the formation to obtain electric fields and complex voltages. The method has an advantage of operating under complicated scenarios including one-, two- and three-layers without knowing the detailed properties.

ACKNOWLEDGEMENTS

I would like to thank my advisor, Dr. Lin Sun for her guidance, inspiration and providing me an excellent environment for conducting research. I would also like to express my gratitude towards the committee members, Dr. Philip C. Munro and Dr. Salvatore R. Pansino for their valued suggestions. I am also very thankful for Dr. Jalal Jalali's guidance and support throughout my studies at YSU. In addition, I would like to thank the professors of Electrical and Computer Engineering department for their teaching and guidance.

I am obliged to Hanna Sassya for his friendly support and helping me during the research. Finally, and most importantly, I would like to thank my family members for their encouragement and endless support during my ups and downs. Without their motivation, I would not have been able to complete this venture.

TABLE OF CONTENTS

ABSTRACT	iii
ACKNOWLEDGEMENTS	iv
TABLE OF CONTENTS	v
LIST OF FIGURES	vii
LIST OF TABLES	xi
LIST OF ABBREVIATIONS	xii
Chapter 1 Introduction	1
1.1 Background	2
1.2 Organization	6
Chapter 2 COMSOL model and implementation of microstrip line	8
2.1 COMSOL model	8
2.2 Four-ports microstrip line	9
2.3 Implementation of microstrip line using COMSOL	11
Chapter 3 EM responses of dipoles in the isotropic Media	19
3.1 EM responses of z-directed coils in a homogenous formation	21
3.2 EM responses of z-directed dipping coils in a homogenous formation	28
3.3 EM responses of z-directed coils in a two-layer formation	33
3.4 EM responses of z-directed coils in a three-layer formation	38
3.5 EM responses of x-directed coils in layered isotropic formation	43
Chapter 4 EM responses of dipoles in the anisotropic Media	50
4.1 EM responses of x-directed coils in a single-layer formation	51
4.2 EM responses of z-directed coils in the anisotropic layered beds	55

4.3 EM responses of x-directed coils in the two-layer formation	60
Chapter 5 Conclusion and future work	65
5.1 Conclusion	65
5.2 Future work	66
References	67

LIST OF FIGURES

Fig. 1 Configuration of three coil	4
Fig. 2 Microstrip	10
Fig. 3 S-matrix for different numbers of port	11
Fig. 4 Design of microstrip line (a) without dielectric, (b) with dielectric	13
Fig. 5 Mesh structure (a) without dielectric, (b) with dielectric	13
Fig. 6 Plot of S-parameters, input at port 1 without dielectric	14
Fig. 7 Plot of S-parameters, input at port 3 without dielectric	15
Fig. 8 EF without dielectric layer	16
Fig. 9 Plot of S-parameters, input at port 1 with dielectric	16
Fig. 10 Plot of S-parameters, input at port 3 with dielectric	17
Fig. 11 EF with dielectric layer	17
Fig. 12 Comparison of S-parameters with port 1 excitation	18
Fig. 13 Profile of a homogeneous formation	22
Fig. 14 3D COMSOL model (a) without a mandrel, (b) with a mandrel	22
Fig. 15 Edge current in transmitter acting as source	23
Fig. 16 Mesh structure	24
Fig. 17 EF distribution without a mandrel	25
Fig. 18 EF distribution with a mandrel	25
Fig. 19 Resistivity versus attenuation	26
Fig. 20 Resistivity versus attenuation	27
Fig. 21 Phase shift versus resistivity	28
Fig. 22 Profile of dipping tool in a homogeneous formation	29

Fig. 23 3D COMSOL model	29
Fig. 24 Mesh structure	30
Fig. 25 Slice view of EF distribution without a mandrel	31
Fig. 26 Attenuation versus resistivity	32
Fig. 27 Phase shift versus resistivity	32
Fig. 28 Profile of a two-layer isotropic media	33
Fig. 29 3D COMSOL model (a) without a mandrel, (b) with a mandrel	34
Fig. 30 Mesh structure without a mandrel	34
Fig. 31 EF distribution without a mandrel	35
Fig. 32 EF distribution with a mandrel	36
Fig. 33 Attenuation versus measured depth	37
Fig. 34 Phase shift versus measured depth	37
Fig. 35 Profile of a three-layer formation	38
Fig. 36 3D COMSOL model	39
Fig. 37 Edge current in transmitter acting as source	39
Fig. 38 Mesh structure with a mandrel	40
Fig. 39 Slice view of EF without a mandrel	41
Fig. 40 Slice view of EF with a mandrel	41
Fig. 41 Attenuation versus measured depth	42
Fig. 42 Phase shift versus depth	43
Fig. 43 Profile of a two-layer isotropic formation	44
Fig. 44 3D COMSOL model (a) without a mandrel, (b) with a mandrel	44
Fig. 45 Mesh structure	45

Fig. 46	Slice view of EF distribution in xy plane without a mandrel	46
Fig. 47	Slice view of EF distribution in xy plane with a mandrel	47
Fig. 48	Attenuation versus measured depth	48
Fig. 49	Resistivity versus attenuation	48
Fig. 50	Phase shift versus measured depth	49
Fig. 51	Profile of a single-layer anisotropic formation	52
Fig. 52	3D COMSOL model without a mandrel	52
Fig. 53	Mesh structure	53
Fig. 54	Slice view of EF distribution without a mandrel	53
Fig. 55	Attenuation versus resistivity	54
Fig. 56	Phase shift versus resistivity	55
Fig. 57	Profile of a two-layer anisotropic formation	56
Fig. 58	Mesh structure without a mandrel	56
Fig. 59	EF distribution without a mandrel	57
Fig. 60	EF distribution with a mandrel	58
Fig. 61	Attenuation versus measured depth	59
Fig. 62	Phase shift versus measured depth	59
Fig. 63	Profile of a two-layer anisotropic media	60
Fig. 64	EF distribution in yz plane without a mandrel	61
Fig. 65	EF distribution in yz plane with a mandrel	61
Fig. 66	Mesh structure	62
Fig. 67	Attenuation versus measured depth	63

Fig. 68 Attenuation versus depth

64

Fig. 69 Phase shift versus measured depth

64

LIST OF TABLES

Table 1 Sources of EM field	1
Table 2 Parameter selection for microstrip line	12

LIST OF ABBREVIATIONS

AC	Alternating Current
dB	Decibel
DOI	Depth of Investigation
ELF	Extremely Low Frequency
EM	Electromagnetic Field
EF	Electric Field
EWFD	Electromagnetic Waves, Frequency Domain
FDM	Finite Difference Method
FDE	Finite Difference Equation
FEM	Finite Element Method
GHz	Gigahertz
HA	High Angle
HZ	Horizontal
IF	Intermediate Frequency
LWD	Logging While Drilling
MD	Measured Depth
MF	Magnetic Field
MHz	Megahertz
MIC	Microwave Integrated Circuit
1D	One Dimensional
RF	Radio Frequency
RR	Receiver-Receiver

3D	Three Dimensional
2D	Two Dimensional
TI	Transversally Isotropic
TR	Transmitter-Receiver

Chapter 1 Introduction

Put simply an electromagnetic field is the combination of an electric field (EF) and magnetic field (MF). An EF is generated by the difference level produce in the voltage whereas an MF is produced by the flow of electric charge, i.e., an EF occurs when the charge is stationary, and MF occurs when the charge is in motion. An EF can be established by a varying MF [1]. An electromagnetic field, also known as an EM field, is created when there is a change in the velocity of an electric charge particle. The history of EM fields is sighted in the 19th century when scientists found that rubbing amber together caused electric sparks and that it could also be regenerated without connecting wires. The first radio transmitter used electric sparks as the salient feature of the communication. EM fields are a form of invisible energy present in the environment. The scattering radiation from thunderstorms is the natural source of the EM fields. X-rays, mobile phone, base stations and power lines are some examples of human-made EM fields [2]. Typical sources of EM fields are shown in Table 1 [3]. EM fields are normally generated by alternating current (AC) in an electric medium. AC is also related to the term called frequency.

Table 1 Sources of EM field

Frequency	Range	Example
Static	0 Hz	Electrolysis
ELF	0 - 300 Hz	Electric engine in vehicles
IF	300 Hz – 100 kHz	Magnetic card reader
RF	100 kHz – 300 GHz	Base transmitting and receiving station

EM logging tools are widely used to measure the resistivity (or conductivity) of earth formations. One of the popular tools is induction logging that operates at low frequency to detect the formation resistivity.

1.1 Background

In oil well logging while drilling, the calculation of earth formation resistivity of different layers by the drill holes has become widely accepted. This method provides a direct contact to the borehole with oil-based mud. An electrode device is used to achieve this as it is associated with insulated electric conductors. The steady current is allowed to flow through the conductor and by ohmic contact method, p.d. (potential difference) is achieved across the conductor that is proportional to the resistivity. The voltage differences in the conductor are carried by the electrode device that measures and records the resistivity at a given time. This is only possible when there is a direct contact made with an electrode device and the mud. But sometimes it is difficult to have ohmic contact between the electrode device and the mud. At this time, it is impossible to get the resistivity by traditional electrical logging tool. This tool needs some extension by the help of a spring, called “scratcher electrode” device which allows the direct contact with the mud formations. Sometimes, we can get the favorable results for the oil wells drilled through hard formation but most of the time it is difficult to get good results due to poor contacts. To overcome the drawback of electrical logging, a new logging tool called “induction logging” is developed. The induction logging tool was first deployed by H. G. Doll in 1949 [4].

Induction logging is invented to calculate earth formation resistivity in boreholes containing oil-based muds and in air-drilled boreholes. The main reason behind the development of induction logging is that the electrode device cannot work in these nonconductive boreholes. However, the induction logging tools are easy to run, and these tools are soon used, in a wide range of borehole salinity, after their invention. The induction logging tools consist of a coil system coupled with the ground by induction. Also, there is now no need for the contact with the mud formation. Due to this reason, induction logging is useful in oil-based muds [6].

In this method, current having certain frequency, i.e., AC is made to flow through a coil, and the coil is referred to as a “transmitter”. This transmitter is supported by an insulating mandrel; then a primary MF is created which generates an eddy current in a transmitter loop. This eddy current follows in a continuous circular path. The secondary MF is created which induces an electromotive force in a secondary coil, and this coil is referred to as a “receiver”. There is certain distance, i.e., spacing between the transmitter and receiver. Since the transmitter current is alternating, there is a phase shift between the transmitter current and the current density in the layer formation. The phase shift is different in all parts of the layer formation; it increases with increase in distance into the layer formation. Also, the phase shift in the receiver is shifted further. At very low conductivity, the total phase shift is nearly 180° and it increases with increasing layer formation conductivity. This is for two coil measurement systems.

For the two coil systems (one transmitter and one receiver), the mutual induction can produce a voltage of several thousand times that provided from a formation. Hence, two coil systems are not widely used these days. The simplest system type is the three

coil measurement systems with one transmitter and two receivers that are more practically in use. In this system, the transmitter is placed on the bottom and at a certain spacing the first receiver is placed, and then the second receiver is arranged above the first receiver. There is a certain fixed TR and RR spacing maintained depending upon the requirement. This type of measurement system is more popular. Fig. 1 shows how the general configuration of the transmitter and receiver are arranged in the induction logging tool.

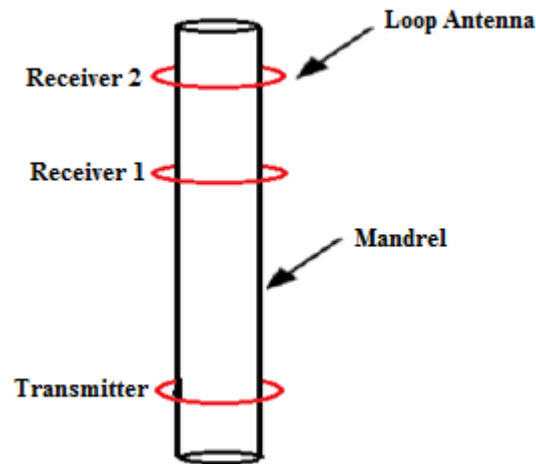


Fig. 1 Configuration of three coil

The resistivity of layer formation transversed by a drill hole can be determined easily by the induction logging tool. This method is useful as the induction logging tool can be moved freely along the drill hole to record the earth formation resistivity, whereas in electrical logging resistivity is obtained only on the base surface of the ground. Also, this type of system is very popular where direct contact with the layer formation is difficult to make [7].

Triaxial induction tools are designed to determine and measure the electrical resistivity parallel and perpendicular to the bedding plane surface. The construction of the transmitter and receiver, used in traditional uniaxial logging, have limited features due to the accuracy of tool response at high resistivity or in deviated wells. To overcome this, triaxial induction logging tool is introduced. The advantage of a triaxial tool is that the resistivity can be measured in three dimensions (triaxially), i.e., x, y and z direction. These logging tools are much more complex, and it also requires fast processing system. Triaxial is composed of two words “tri” which means “three” and “axial” which means “axes”. Triaxial measurement tool has three sets of coils; one transmitter coil and two receiver coils. Triaxial transmitters and receivers may be fabricated in the time domain or frequency domain [8].

The tool axis may intercept a formation with dip angle, azimuthal angle and orientation angle. Since there are three sets of transmitters and receivers, EM fields are generated by these three transmitters, resistivities are then calculated by using three receivers. The triaxial transmitter coil generates 3D EM fields in three different directions, and each triaxial receiver coil has a directly coupled term and two cross-coupled terms with the transmitter coils in other directions. So this leads to nine terms in a 3×3 voltage matrix array for any given measurement, i.e., H_{xx} , H_{xy} , H_{xz} , H_{yx} , H_{yy} , H_{yz} , H_{zx} , H_{zy} , and H_{zz} .

$$H = \begin{bmatrix} H_{xx} & H_{xy} & H_{xz} \\ H_{yx} & H_{yy} & H_{yz} \\ H_{zx} & H_{zy} & H_{zz} \end{bmatrix} \quad (1.1)$$

The term H_{ij} denotes the MF measured by the j-receiver from i-transmitter. All these nine couplings are measured simultaneously. The axis of the tool may intercept a

formation with dip and azimuthal angle. For a transversally isotropic (TI) anisotropic formation with dip but no strike, i.e., zero azimuthal angle, the MF components H_{xy} , H_{yx} , H_{yz} , H_{zy} vanishes. The azimuthal angle is constructed again by discarding the azimuthal angle at which the data tensor can be rotated to minimize the cross-coupling components of the MF for each TR spacing [9].

An advanced inversion method extracts resistivity anisotropy, bed boundary positions and relative dip angle from the voltage tensor matrix, and the receiver arrays are located at different spacing to prove multiple depth of investigation (DOI). Responses on a triaxial system can be categorized into three aspects: coaxial, coplanar and cross components. This coplanar component plays a significant role in determining an anisotropic resistivity whereas cross component gives a contribution to detect the formation bed. The inversion approach helps to regulate dipping angle based on both coplanar and cross components.

The traditional axial induction tool is limited and is not able to detect anisotropy formation. This triaxial measurement system guides to overcome the problem by having three mutually perpendicular transmitter and receivers, and are capable of collecting electrical information from every direction [5, 21].

1.2 Organization

This thesis is divided into five chapters. Chapter 1 includes the brief introduction about the induction logging tool along with the history and development of induction logging tool. Chapter 2 gives the overview of COMSOL and implementing it to investigate S-parameters of 4-port microstrip line. Chapter 3 covers the EM response of

z-directed and x-directed coils in the isotropic formations. Chapter 4 deals with the study of EM response of z-directed and x-directed coils in the anisotropic formations. Finally, Chapter 5 provides the conclusion and future enhancement of this work.

Chapter 2 COMSOL model and implementation of microstrip line

This chapter covers the basic description of COMSOL and the way to investigate the S-parameters for the four-port microstrip line.

2.1 COMSOL model

In 1986, COMSOL Multiphysics was originally started by the duo of graduate students in Stockholm, Sweden at the Royal Institute of Technology (KTH) as a part of their project. COMSOL is an interactive tool used to model and solve all kinds of engineering problems. This tool provides powerful unified desktop surroundings with a model builder, which gives the full analysis of the model and access to all the integrated functions. The main task is solving problems that involve coupled physics phenomena, which are also known as a multiphysics, i.e., model for one type can be extended into multiphysics model. The COMSOL software consists of various combined workflow for electrical, mechanical and chemical applications [10].

The model builder contains two parts, one is the physics builder and another one is an application builder. The physics builder allows the user to create a custom made physics interfaces attainable from COMSOL Multiphysics, which looks like a similar built-in interface. The model can be made by using new interface component from the tree structure of physics. No programming is required as it works in COMSOL Multiphysics from the physics tree. The application builder allows saving a model as a special application. For designing applications, two editors are available, form editor and method editor. In the form editor, drag and drop tools are used whereas in the method editor, the programming part is done. There are also ways of integrating it with

MATLAB, which increases the possibilities. One of the significant features of this tool is the ability to put the equations as needed in the form of differential equations. This is quite useful as different equations used in the physics, to describe a system, are differential equations.

COMSOL summons and solves the model using a set of numerical analysis tool. It has grown much over the years and continues to be crucial software not only in solving the problems but also in visualizing. COMSOL Multiphysics establishes mechanism to record all the steps that design the geometry, mesh, materials, studies and visualization and result presentation. This helps to parameterize the model by simply changing the node in the model tree and re-running the simulation [11].

2.2 Four-ports microstrip line

Microstrip line is one type of transmission line that is used to transport microwave frequency signals from one electric medium to another. Microstrip transmission lines have been widely used in microwave integrated circuit (MIC) and is composed of a conductor and a ground plane separated by a dielectric substrate. It can be used to build the component like antennas, filters and couplers. Transmission characteristics of microstrips are explained by two parameters, effective dielectric constant and characteristic impedance. The positive aspects of using a microstrip are they are cheaper, weigh less and are more concentrated than the other waveguides. It is the most popular microwave transmission line structure used for the measurement of voltages, currents and waves. They are widely used in the manufacture of integrated semiconductor form. The negative aspects include the fact that they cannot handle high power and are vulnerable to

cross talk as they are open devices. When high isolation is needed some supportive shield, in the form of a filter or switch, is required. In a microstrip line, some portion of EM fields exists in the air above the dielectric substrate and some within the dielectric substrate itself. Generally, the dielectric constant of the line is greater than that of air and less than that of a substrate. A simple diagram of microstrip is shown in Fig. 2, with A as wire strip (conductor), B as a dielectric (usually air), D as a ground plate, C as a substrate that separates the conductor and ground plate [12].

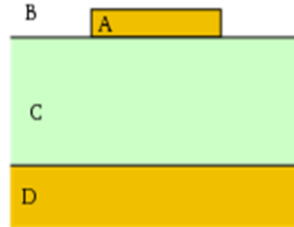


Fig. 2 Microstrip

With the help of COMSOL Multiphysics, S-parameters of a model can be calculated. In S-parameters, “S” stands for “scattering”, and are usually organized into a matrix known as S-matrix (scattering matrix). This matrix helps for the computation of RF energy propagation through a multi-port model. The purpose of the matrix is to define how the signals interact within a system. There is requirement for the system to be simplified because some of the signals will bounce out of the port that it came from, some of it penetrates through the other ports, and some of it disappears as a loss. S-matrix helps to consider all the input-output possibilities of the signal. One thing to keep in consideration is these parameters are complex numbers because both the magnitude and

phase of the signal are changed by the system. But the magnitude of the signal is considered only, as it is of more practical concern. The S-parameters changes with the frequency and impedance of the system. Fig. 3 shows how S-matrices can be used for one-, two-, and three-port networks [13].

$$\begin{aligned}
 & (S_{11}) \quad (\text{one-port}) \\
 & \begin{pmatrix} S_{11} & S_{12} \\ S_{21} & S_{22} \end{pmatrix} \quad (\text{two-port}) \\
 & \begin{pmatrix} S_{11} & S_{12} & S_{13} \\ S_{21} & S_{22} & S_{23} \\ S_{31} & S_{32} & S_{33} \end{pmatrix} \quad (\text{three-port})
 \end{aligned}$$

Fig. 3 S-matrix for different numbers of port

S-matrix has a form of S_{ij} , the first term “i” stands for responding port while the second term “j” represents the incident port, i.e., term “i” is the output port and term “j” is input port. Thus, the signal goes from the j-port to i-port. When the term “i” is equal to the term “j”, i.e., diagonal parameters, they are referred as transmission coefficients. The S-parameters become ratios of input and output voltages.

2.3 Implementation of microstrip line using COMSOL

In COMSOL, under model wizard, a 3D model is picked under which radio frequency > electromagnetic waves, frequency domain (EWFD) is selected then in preset studies, frequency domain is set. The next step in the design is to set the parameters for

the model which include length and width of the ground plane, dimension of the metal lines, distance of the lines from the ground plane, thickness of the ground plane and metal lines and distance between metal lines. These parameters are included by locating the parameter section under home toolbar as shown in Table 2

Table 2 Parameter selection for microstrip line

Name	Expression	Description
L	10 [mm]	Length of microstrip
W	5[mm]	Width of microstrip
T	0.05[mm]	Thickness of ground plane
D	0.3[mm]	Distance between metal lines and ground plane

When the model design is complete, necessary physics are added. The first step is to apply the perfect electric conductor boundary condition to the interior boundaries of the microstrip lines, and then the four lumped ports are added to the model using the physics toolbar. The model is simulated into two parts, without dielectric and with dielectric. The model are designed in COMSOL as shown in the Fig. 4 by using these parameters. For the first part, the wave excitation is turned on at the first port then material properties are assigned to the model. These materials include air that is inside the built-in function window “add material” and the conductivity of the material for the metal line is 5.8×10^7 S/m, which is the same value as pure copper.

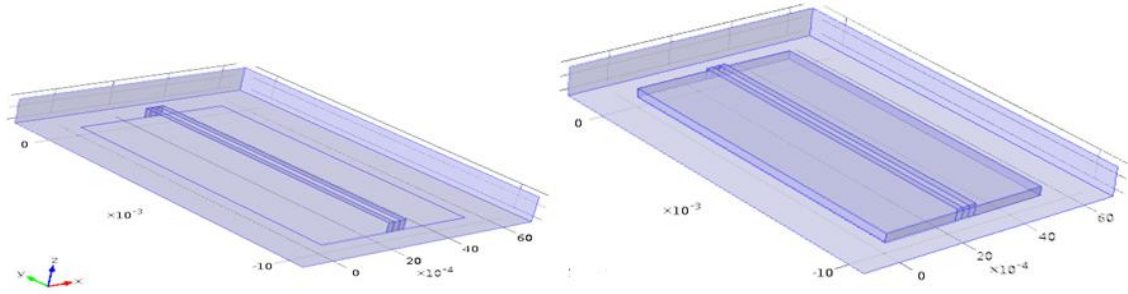


Fig. 4 Design of microstrip line (a) without dielectric, (b) with dielectric

The target is to observe the EF in the metal lines, so small mesh, i.e., fine mesh is picked in order to maximize the sampling of the simulation. Fig. 5 shows the mesh structure used for the simulation.

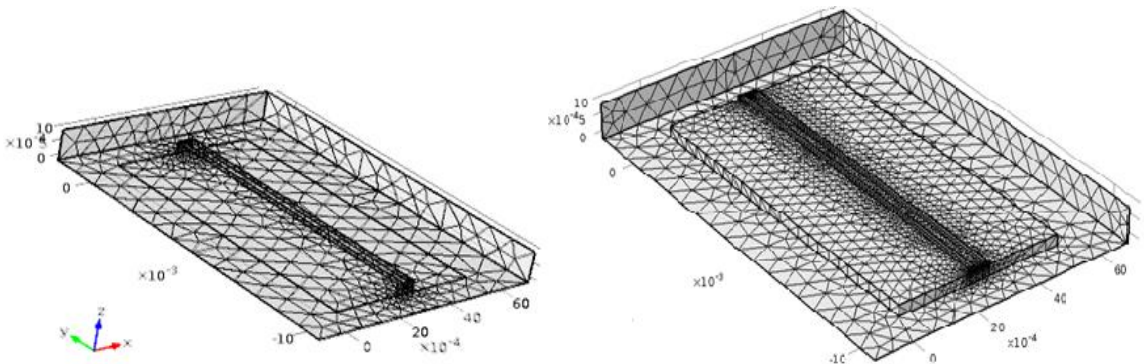


Fig. 5 Mesh structure (a) without dielectric, (b) with dielectric

As we move out to the boundary of the model, the size of the mesh gets much larger. After the mesh structure is created, the frequency range is selected from 0 to 1 GHz in frequency domain under study window. The only difference between the model

without and with dielectric is the addition of dielectric material with the relative permittivity of 2.6. For the S-parameters, wave excitation of port 1 and port 3 is turned on and then “add expression” is selected under global setting window. The simulation of S-parameters S_{11} , S_{21} , S_{31} , S_{41} and S_{13} , S_{23} , S_{33} , S_{43} are done to get the values. The first subscript is the output port, and the second subscript is the input port. Fig. 6 and Fig. 7 show the S-parameter plot for first part, i.e., without dielectric.

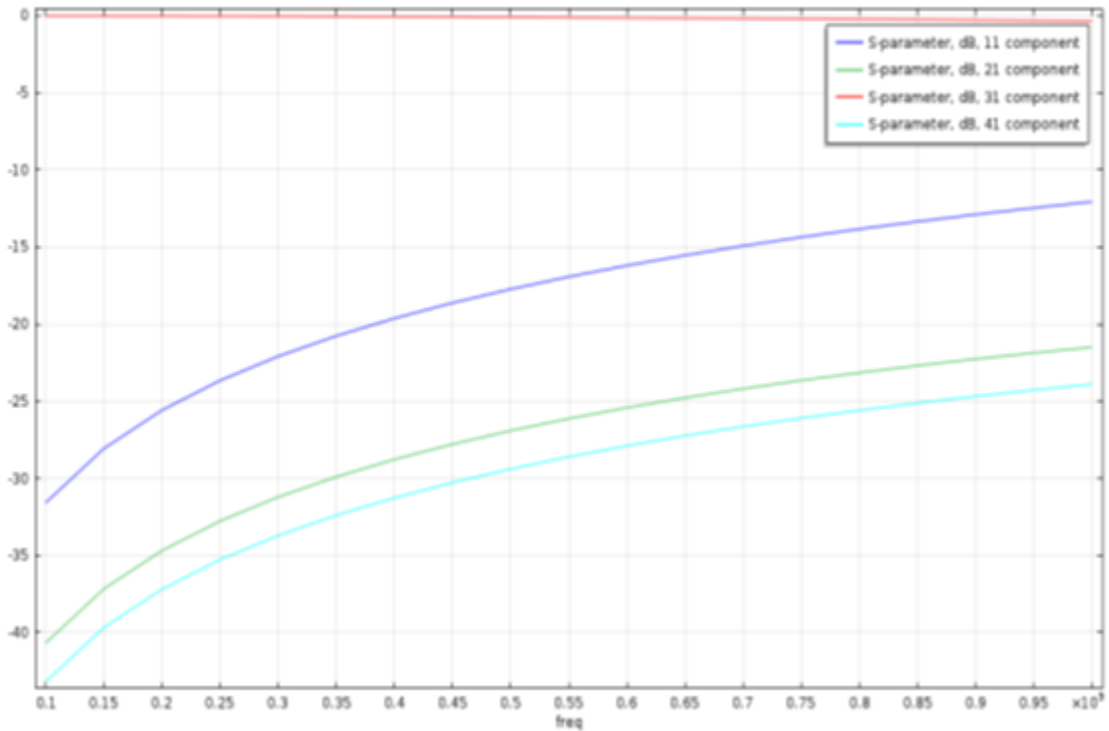


Fig. 6 Plot of S-parameters, input at port 1 without dielectric

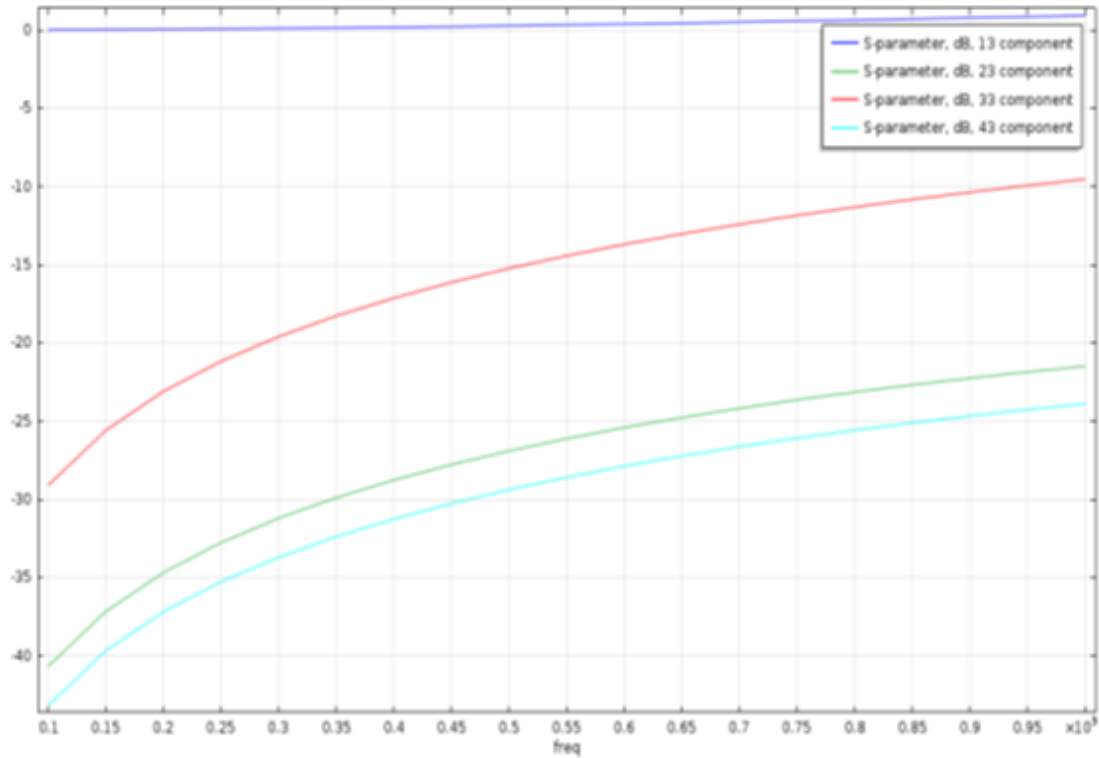


Fig. 7 Plot of S-parameters, input at port 3 without dielectric

From these plots, we can see that the parameters S_{13} and S_{31} are just opposite of each other. This is what one should expect from the matrix of S-parameters. Also, the S-parameters are reliant upon the frequency and there is the variation of frequency from 0.1 to 1 GHz. Fig. 8 shows the strength of the EF traveling along the metal line strips for the case without dielectric.

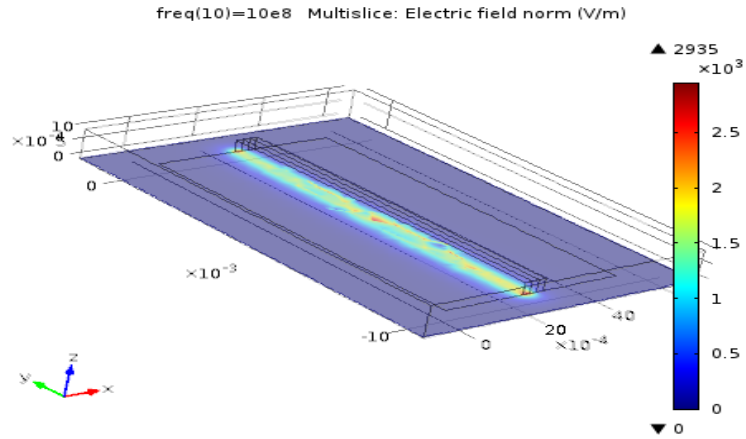


Fig. 8 EF without dielectric layer

Same process is used for the simulation of microstrip line with the addition of dielectric. The S-parameter plots with dielectric case are shown in the Fig. 9 and Fig. 10 respectively, with Fig. 11 showing the EF strength traveling along metal lines.

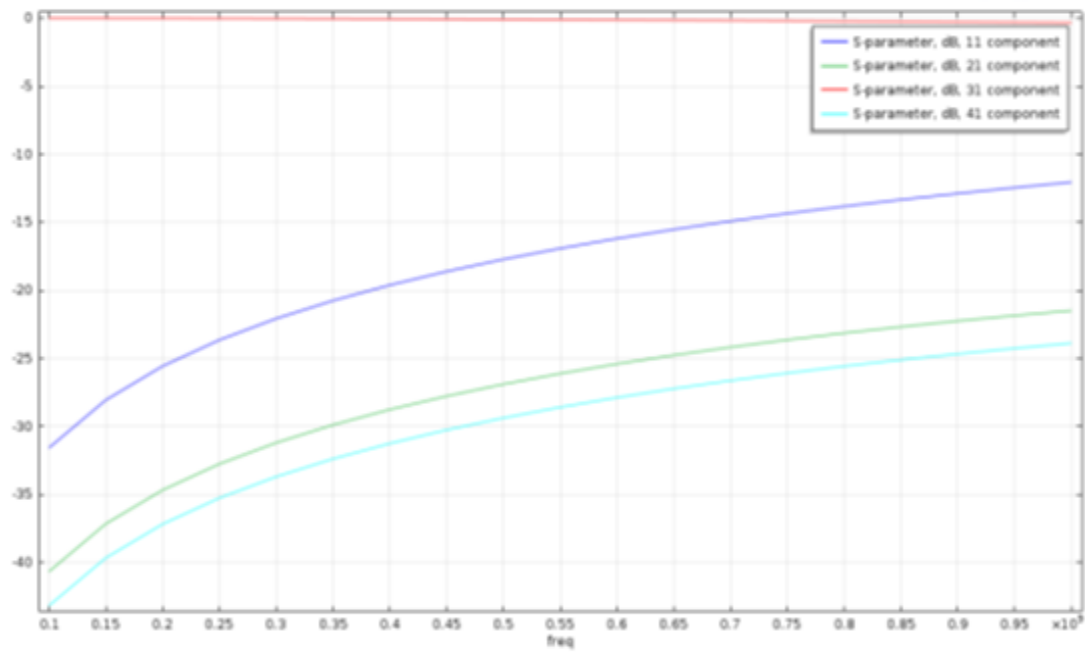


Fig. 9 Plot of S-parameters, input at port 1 with dielectric

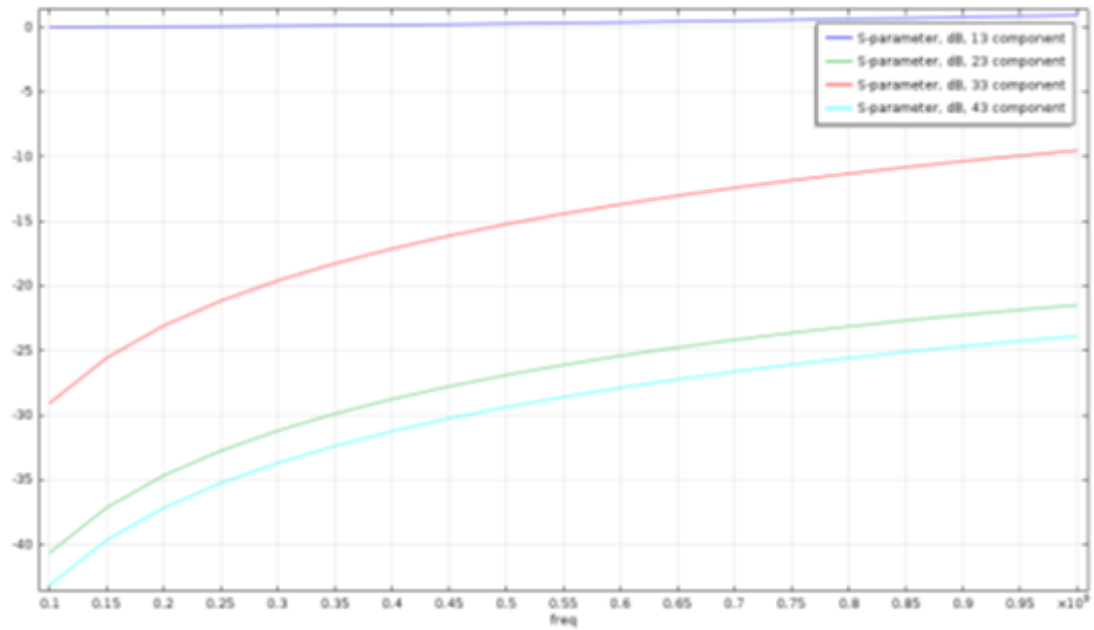


Fig. 10 Plot of S-parameters, input at port 3 with dielectric

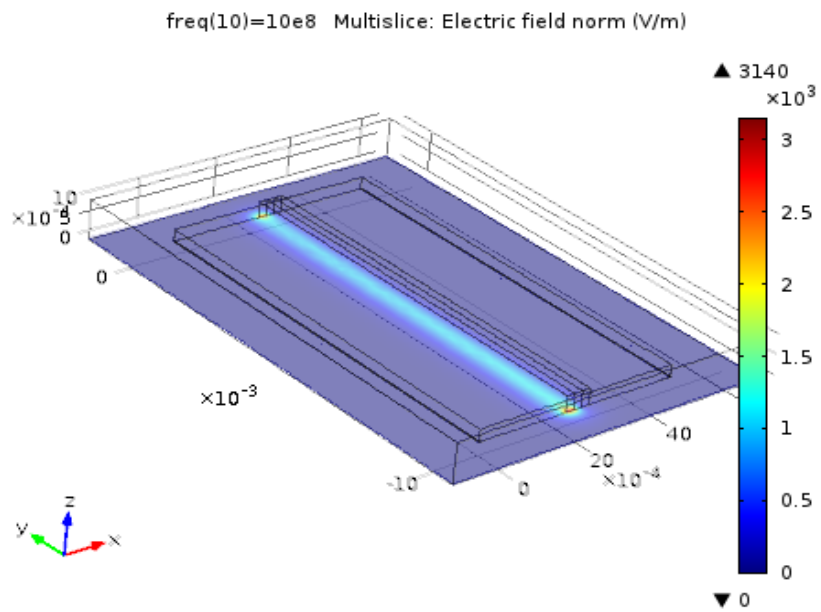


Fig. 11 EF with dielectric layer

Fig. 12 shows the comparison of S-parameter plot of port 1 for both parts. There is a slight offset created by the dielectric layer, but these plots look identical. The addition of dielectric material between the ground plane and metal strips has a negligible effect on the S-parameters and does not affect the voltage transmission across the metal strips.

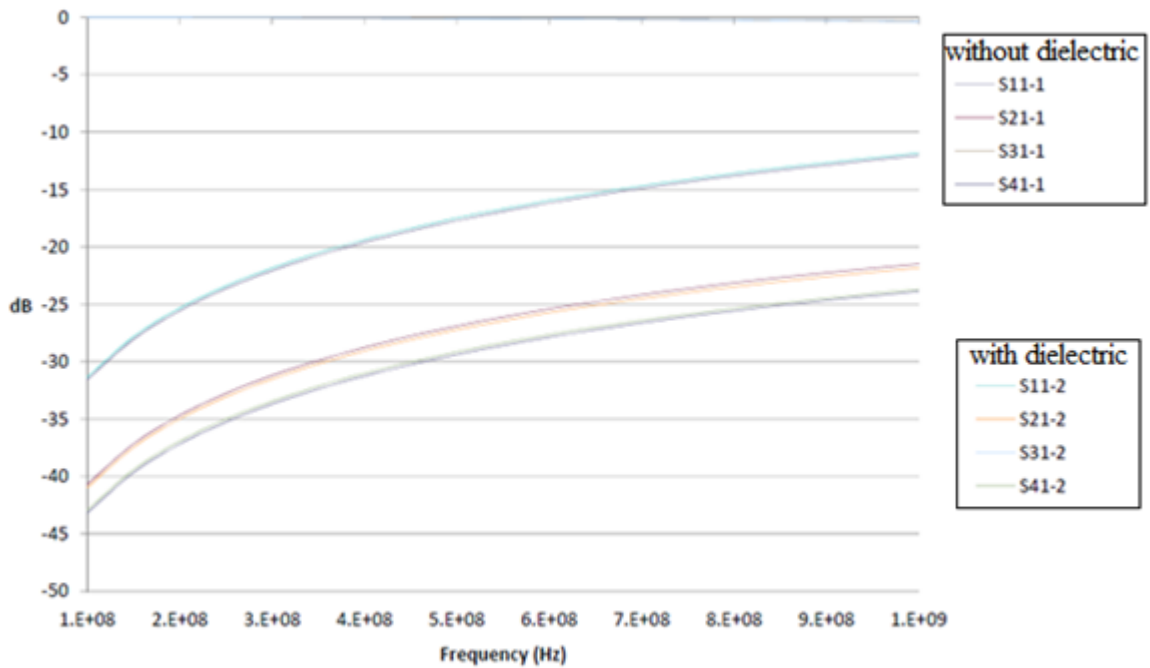


Fig. 12 Comparison of S-parameters with port 1 excitation

Chapter 3 EM responses of dipoles in the isotropic media

Maxwell's equation in electromagnetic waves, frequency domain (EWFD) interface for RF module is expressed as

$$\nabla \times \mu_r^{-1} (\nabla \times \mathbf{E}) - \omega^2 \epsilon_o \mu_o \left(\epsilon_r - j \frac{\sigma}{\omega \epsilon_o} \right) \mathbf{E} = 0 \quad (3.1)$$

The EWFD speculates that the resultant EM fields are obtained from the radiation. This speculation can achieve both near-field as well as far-field radiations around transmission lines, antennas and resonant coils. Another method is using the equation for MF in the frequency domain which is given by the relation

$$\nabla \times \mu^{-1} (\nabla \times \mathbf{A}) + (j\omega\sigma - \omega^2 \epsilon) \mathbf{A} = \mathbf{J}_s \quad (3.2)$$

This equation (3.2) corresponds to MF.

The EF \mathbf{E} is related to magnetic vector potential by the equation

$$\mathbf{E} = j\omega\mathbf{A} \quad (3.3)$$

The induced current density \mathbf{J}_i is related to the EF by the equation

$$\mathbf{J}_i = \sigma\mathbf{E} \quad (3.4)$$

Here \mathbf{E} , \mathbf{A} , \mathbf{J}_s and \mathbf{J}_i represents EF, magnetic vector potential, source current density and induced current density respectively, EF and induced current are solved after the MF is known. The MF frequency domain is mostly used for the “quasi-static” field. This speculation can achieve only near field radiation like current induced in metallic objects near current carrying conductor [14].

Consider EF and MF medium to be a sinusoid, which is represented by the following equations

$$\mathbf{E}(x, y, z, t) = \mathbf{E}(x, y, z)e^{j\omega t} \quad (3.5)$$

$$\mathbf{H}(x, y, z, t) = \mathbf{H}(x, y, z)e^{j\omega t} \quad (3.6)$$

Combining these two equations into a time harmonic equation, we get

$$\nabla \times (\mu^{-1} \nabla \times \mathbf{E}) - \omega^2 \epsilon_c \mathbf{E} = 0 \quad (3.7)$$

$$\nabla \times (\epsilon_c^{-1} \nabla \times \mathbf{H}) - \omega^2 \mu \mathbf{H} = 0 \quad (3.8)$$

This equation (3.7) is generally taken into consideration for EWFD user interface. Also, using the relation $\epsilon_r = n^2$, where n = refractive index, the equation (3.7) can be conversely written as

$$\nabla \times (\nabla \times \mathbf{E}) - k_0^2 n^2 \mathbf{E} = 0 \quad (3.9)$$

where $k_0 = \sqrt{\epsilon_0 \mu_0} = \frac{\omega}{c_0}$ is wave number in vacuum and c_0 is the speed of light in vacuum [15].

Two different methods, EM solver and MF solver are used to compute complex voltages at the receivers. EM solvers are special purpose programs that incorporate Maxwell's equation, and they can be the form of either boundary discretization or domain discretization methods. Like EM solvers, MF solvers are also special computer program that determines the MF generated from the EM coils. These EM and MF solvers iteratively solves the finite difference equation (FDE) to determine the respective electric and magnetic potentials and can be used to solve the 2D and 3D problems [16, 17]. To obtain the voltage, line integral is computed shown in the following equation below which gives the relationship between voltage and EF. This is used in the EM solver.

$$v = \oint_c \mathbf{E} \cdot \hat{\mathbf{t}} dl \quad (3.10)$$

The EF vector components at edges are available as tEx , tEy and tEz and the edge tangent vector is denoted by $t1x$, $t1y$ and $t1z$ respectively. This projection tE is defined by the dot product of the EF and the tangent vector to the EF.

$$\mathbf{E} \cdot \mathbf{t} = tEx * t1x + tEy * t1y + tEz * t1z \quad (3.11)$$

The voltages are evaluated at both receivers, i.e., V_1 for the first receiver and V_2 for the second receiver, attenuation and phase shift are calculated by the using following equations

$$\text{Att} = 20 \log_{10} \frac{|V_1|}{|V_2|} \quad (3.12)$$

$$\text{Phase Shift} = [\theta (V_1) - \theta (V_2)] \quad (3.13)$$

For MF solver, line integral is computed shown in the following equation

$$v = i \omega \oint_c \mathbf{A} \cdot \hat{\mathbf{t}} dl \quad (3.14)$$

where $\mathbf{A} = (A_x, A_y, A_z)$ is magnetic vector potential

3.1 EM responses of z-directed coils in a homogenous formation

Fig. 13 shows the profile formation of a single-layer homogenous medium. The model is designed with and without a mandrel. A large block is selected, so the boundary is far away from the tool that is put in the center. The material properties are electric conductivity (σ) of 0.0056 S/m, relative permittivity (ϵ_r) of 53.4652 and relative permeability (μ_r) of 1. A finite size transmitter and two receiver loop antenna are used having the radius of 4.5 inches with TR spacing of 28 inches and RR spacing of 6 inches. Dielectric material is related with conductivity by the following equation

$$\epsilon_r = 108.5 * \sigma^{0.35} + 5 \quad (3.15)$$

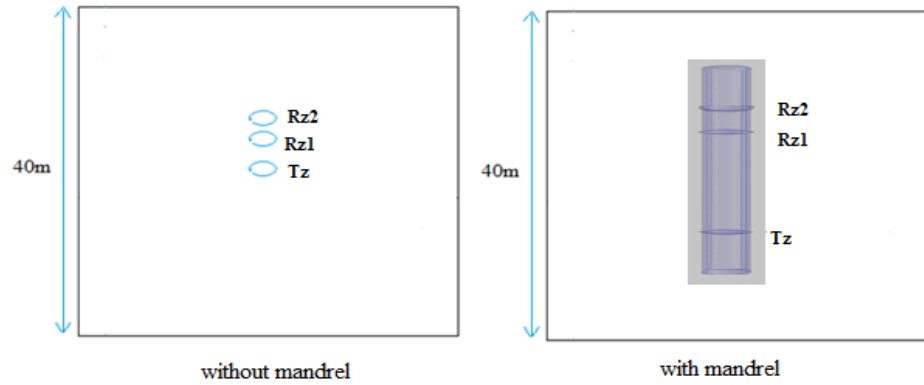


Fig. 13 Profile of a homogeneous formation

The scattering boundary condition is set to the outer boundary. Also, we can use impedance boundary at the edge of an overall domain so as to limit the size to simulation domain. The cases we used are a finite size antenna, and they are not axis symmetrical. Fig. 14 shows the 3D models used for the design for a single-layer formation for both cases without and with a mandrel, and the calculations on these 3D models will be conducted using COMSOL.

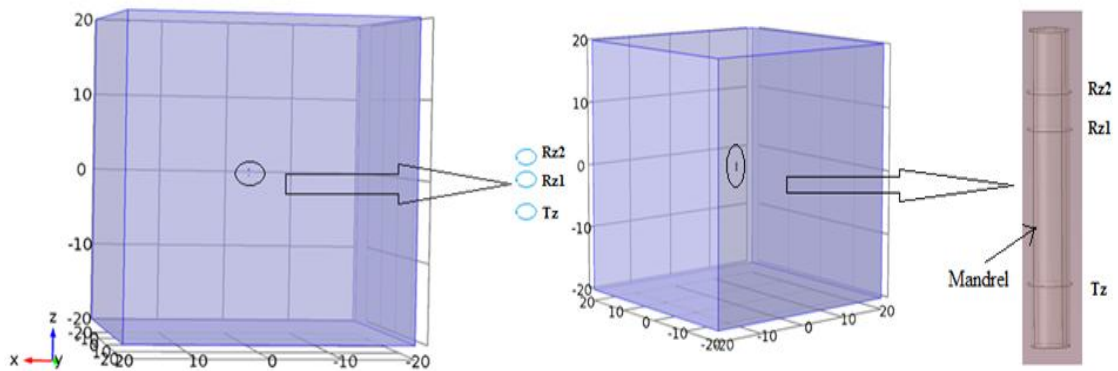


Fig. 14 3D COMSOL model (a) without a mandrel, (b) with a mandrel

The three circles represent one transmitter and two receivers, with a cylinder representing the metallic mandrel. The metallic mandrel used is steel having a radius of 4 inches and height of 51 inches with $\sigma = 0.1$ S/m, $\epsilon_r = 20$ and $\mu_r = 1200$. A line source of 1A current is assigned to the loop used as transmitter, and complex voltages are calculated on two receivers respectively to obtain attenuation and phase shift. Both the transmitter and receivers are z-directed magnetic dipoles. An edge current is used to excite the transmitter; the transmitter and receiver are modeled as finite size loop with an infinitesimal thin wire. Here, edge current in the transmitter coil side acts as a source shown in the Fig. 15.

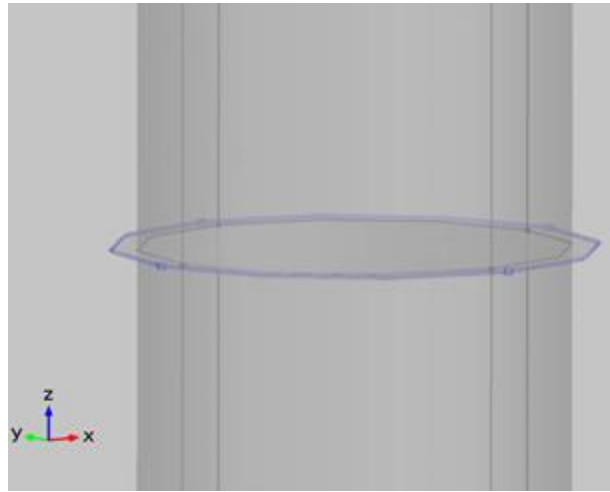


Fig. 15 Edge current in transmitter acting as source

Normal mesh size is used with the maximum element size value of 4 m and minimum element size value is 0.72 m and same mesh is used for the cases without and with a mandrel. Fig. 16 shows the mesh structure, and the number of tetrahedral elements are found to be 17,976 and 18,703 respectively for the cases without a mandrel and with a

mandrel. It is obvious that the number of elements is more in the latter case because of the extra element, “mandrel”.

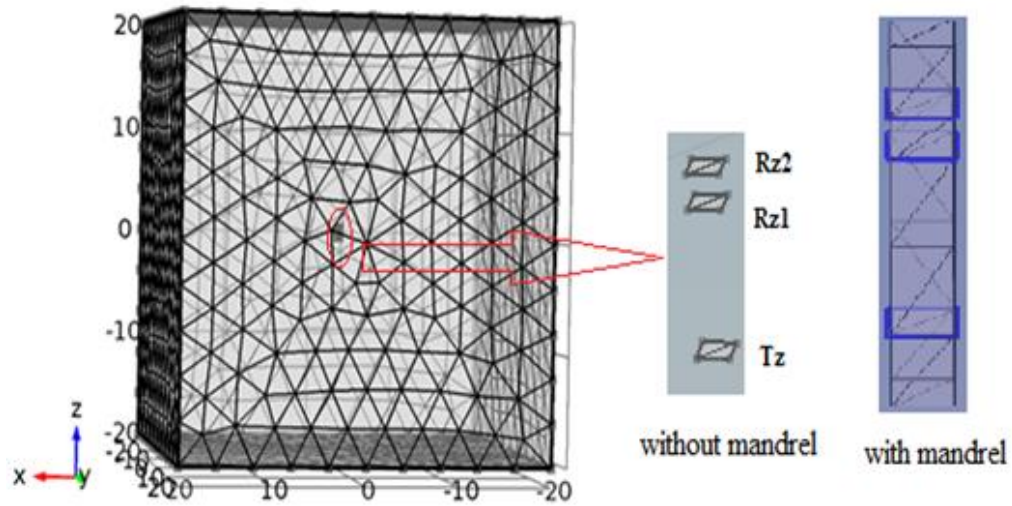


Fig. 16 Mesh structure

Here, the scattering boundary condition is set to the outer boundary. Fig. 17 and Fig. 18 show the EF distribution using EM solver at $\sigma = 0.0056$ S/m from a z-directed transmitter of logging while drilling (LWD) propagation resistivity, operating at the frequency of 2 MHz in a homogeneous medium using COMSOL. In Fig. 17, there is presence of strong EF between the range -20 to -40 dB, this is the case without using a mandrel. Looking onto the Fig. 18, EF is strong between the range 0 to 20 dB. There is an increase in gain due to the presence of a mandrel.

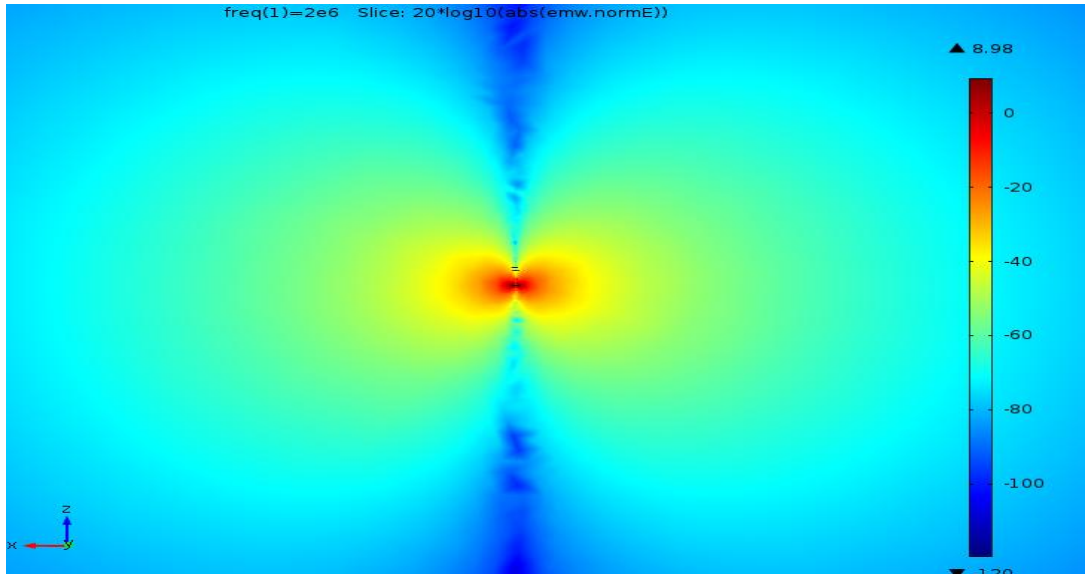


Fig. 17 EF distribution without a mandrel

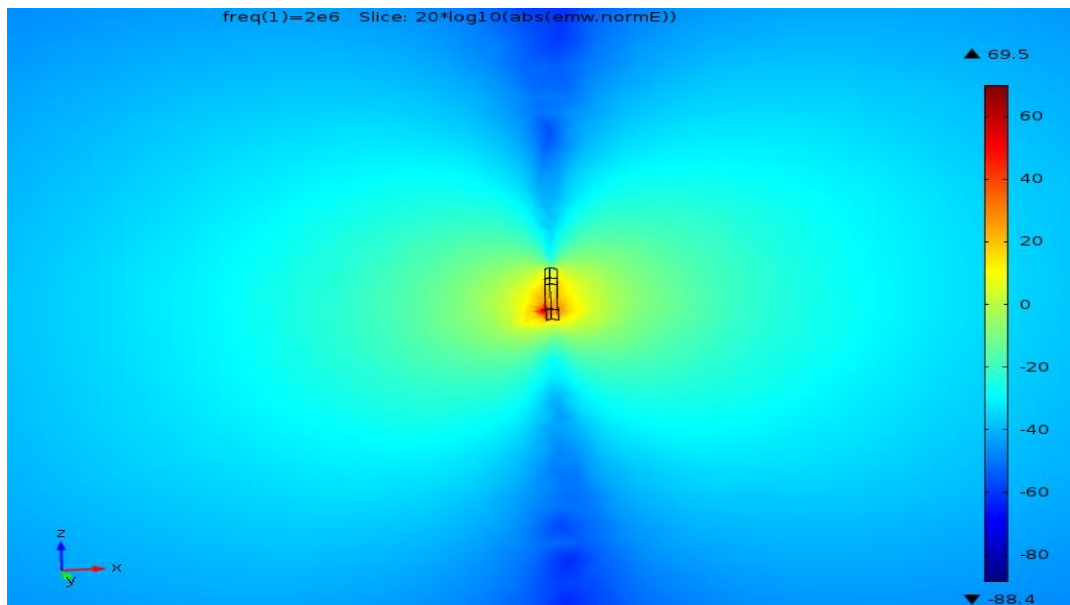


Fig. 18 EF distribution with a mandrel

Simulation is performed with the conductivity varying from 0.005 to 5 S/m. For the case without a mandrel, the memory size is approximately 785 MB with the run time of 180 sec whereas it takes more memory size for the case with a mandrel, which is found to be approximately 1.2 GB with the run time of 270 sec. The attenuation and phase shifts are plotted using MATLAB with Fig. 19 showing the characteristic plot of formation resistivity versus attenuation.

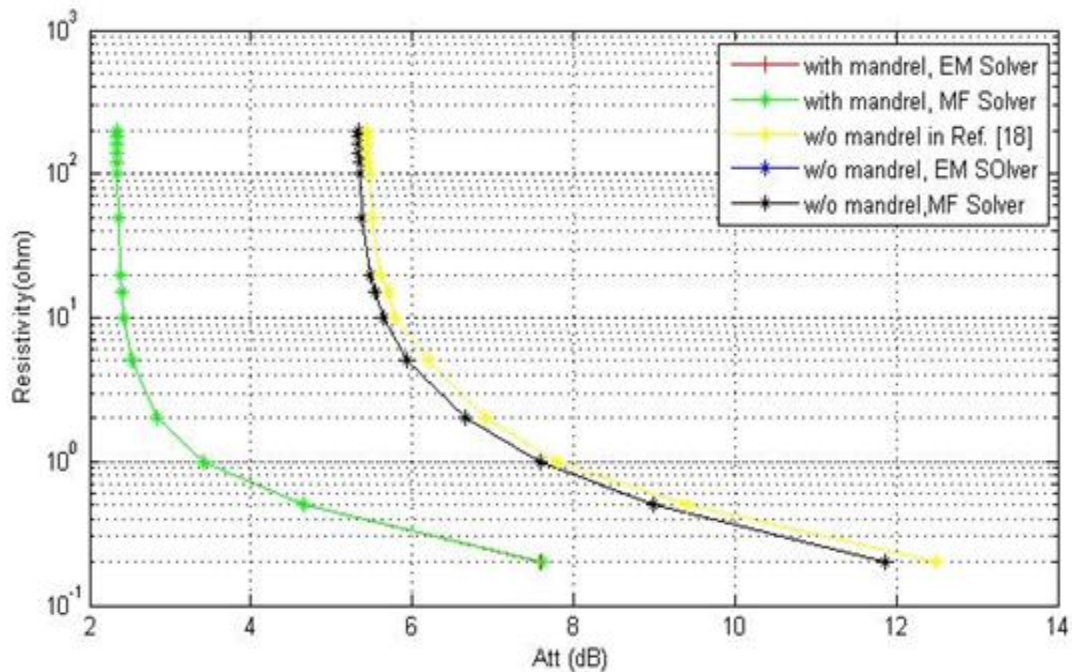


Fig. 19 Resistivity versus attenuation

For EM and MF solver without using a mandrel there is a slight change making mesh structure from normal to extra fine keeping the normal mesh for the case with a mandrel. In Fig. 19, we can see that the result from the COMSOL 3D models and results from the reference value almost agree. Comparing these plots, at the resistivity of 0.2 Ω ,

attenuation is found to be 12.3 dB for reference and 11.9 dB from COMSOL 3D for EM solver and MF solver without a mandrel. Similarly, at the resistivity of 5 Ω , attenuation is 6.2 dB and 6 dB respectively. For the resistivity of 20 Ω , attenuation is 5.6 dB and 5.5 dB. For the resistivity of 100 Ω , attenuation is 5.48 dB and 5.46 dB. The graph is slightly off by 0.3 dB when compared with the reference results. The most important thing to be considered is the size of the mesh; the finer mesh, the closer the reference result. Fig. 20 shows the resistivity versus attenuation plot of a reference result.

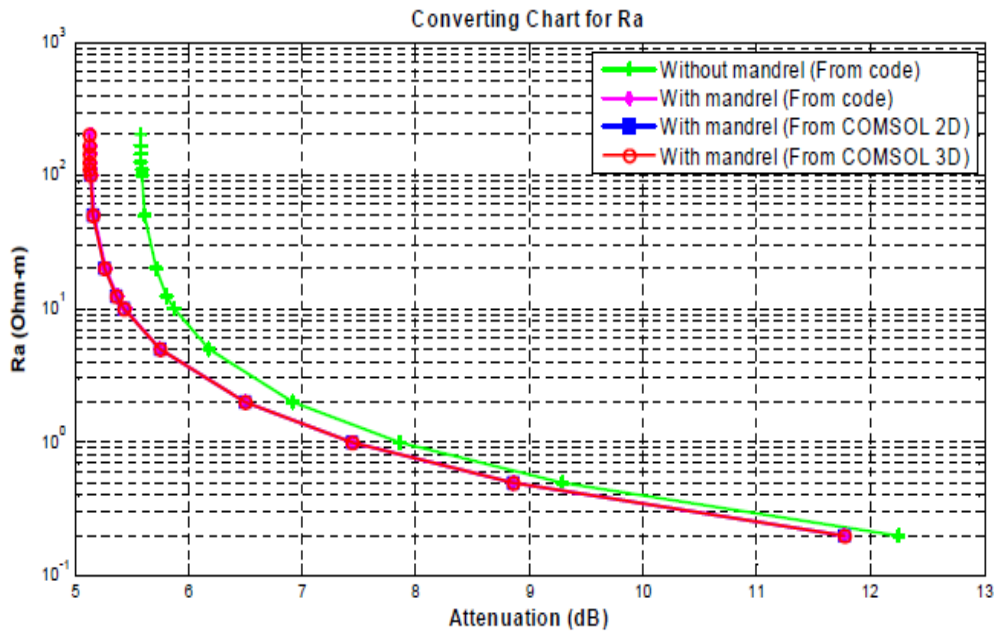


Fig. 20 Resistivity versus attenuation (from Ref. [18])

Also, with the presence of a mandrel in the model there is a downward shift in the attenuation and upward shift in the phase. The characteristics plot of phase shift versus formation resistivity is shown in the Fig. 21.

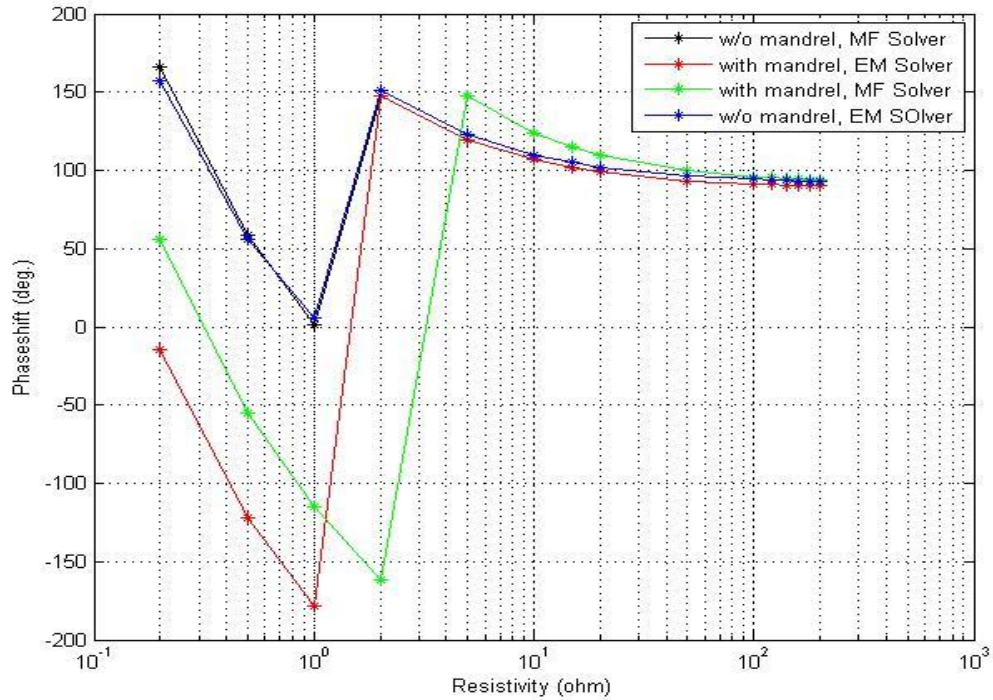


Fig. 21 Phase shift versus resistivity

3.2 EM responses of z-directed dipping coils in a homogeneous formation

For dipping tool in a homogeneous medium, the model is designed without using a mandrel. A finite size transmitter and two receiver loop antenna are used having a radius of 4.5 inches with TR spacing of 28 inches, and RR spacing of 6 inches is used for the design. Also, all the transmitters and receivers are z-directed. The material used for the block have following property as $\sigma = 0.005$ S/m, $\epsilon_r = 1$ and $\mu_r = 1$. The electric conductivity is varied from 0.005 to 5 S/m. This homogeneous case is studied with the dipping angle at 60° and the single-layer material is used. Fig. 22 shows the profile formation for the given model.

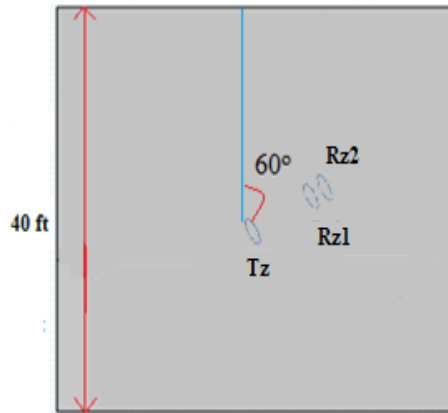


Fig. 22 Profile of dipping tool in a homogeneous formation

A line source ($I = 1A$) is assigned to the loop used as transmitter and complex signals are calculated on the two receivers, and then convert the phase shift and amplitude ratio of these two signals to attenuation resistivity and phase shift resistivity. The 3D COMSOL model for this formation layer is shown below in Fig. 23.

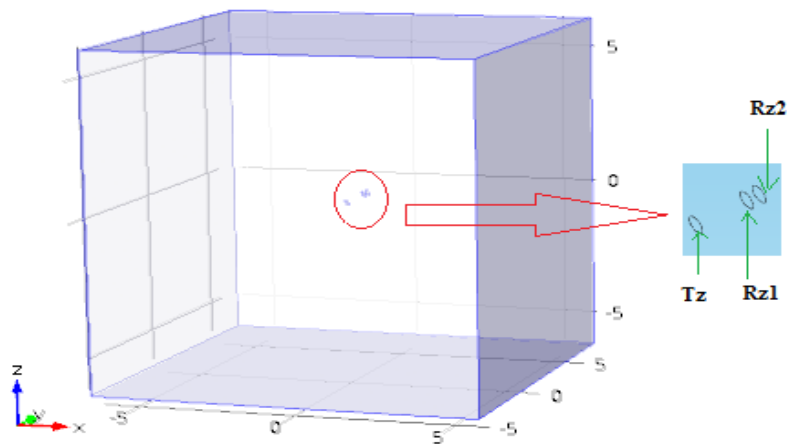


Fig. 23 COMSOL model

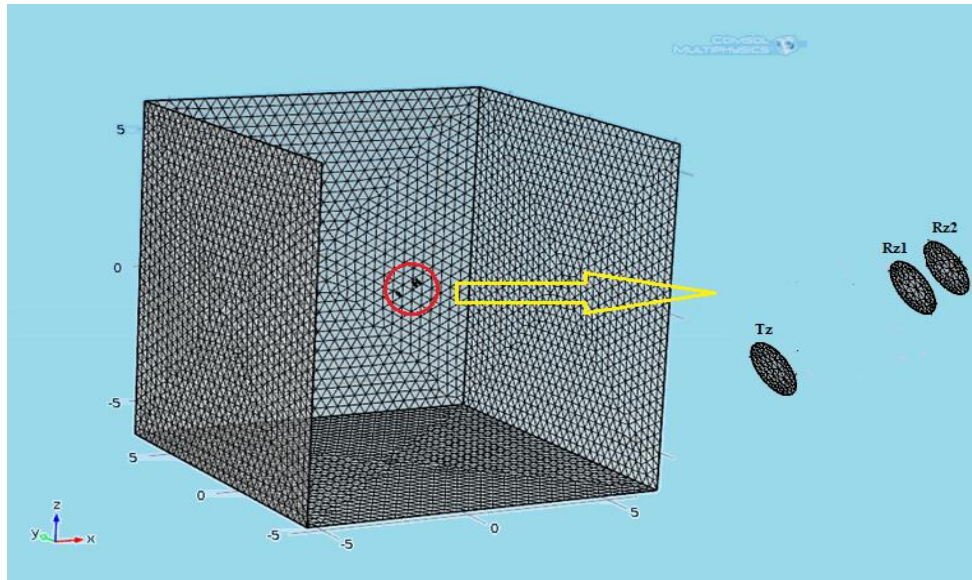


Fig. 24 Mesh structure

Fig. 24 shows the extra-fine mesh structure used for the design of the model. The number of tetrahedral elements is found to be 418,903 with the maximum element size of 0.427 m. EM field is created at the operating frequency of 2 MHz and scattering boundary condition is set to the outer boundary. The EF distribution without a mandrel using EM solver generated at $\sigma = 0.005$ S/m is shown in the Fig. 25, and there is a presence of strong EF at -20 dB.

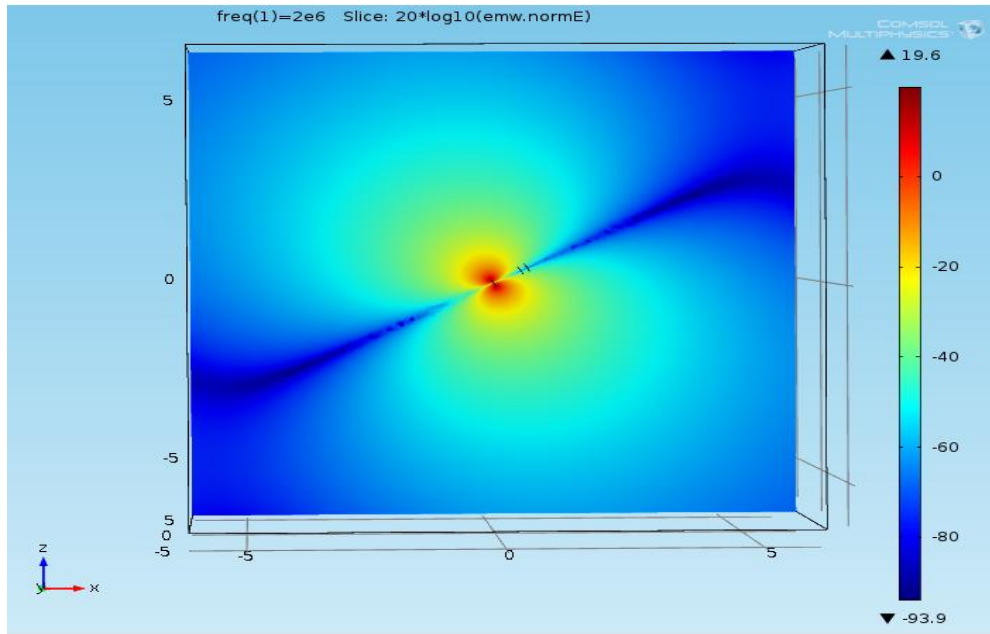


Fig. 25 Slice view of EF distribution without a mandrel

Here, the simulation is performed with the conductivity varying from 0.005 to 5 S/m. The memory size taken for the simulation is 1.44 GB with the total run time for 15 points is found out to be 5,454 sec. The characteristics plots of attenuation and phase shift versus resistivity is plotted using EM solver and MF solver are shown below in the Fig. 26 and Fig. 27 respectively. The attenuation plot and phase shift plot are similar for both solvers. At resistivity of 0.2Ω , attenuation is about 11.9 dB and 11.7 dB and phase shift is close to 160° respectively for EM and MF solver and at other values of resistivity these two plots look similar. Even for other values of resistivity, attenuation and phase shift are very close for EM and MF solvers.

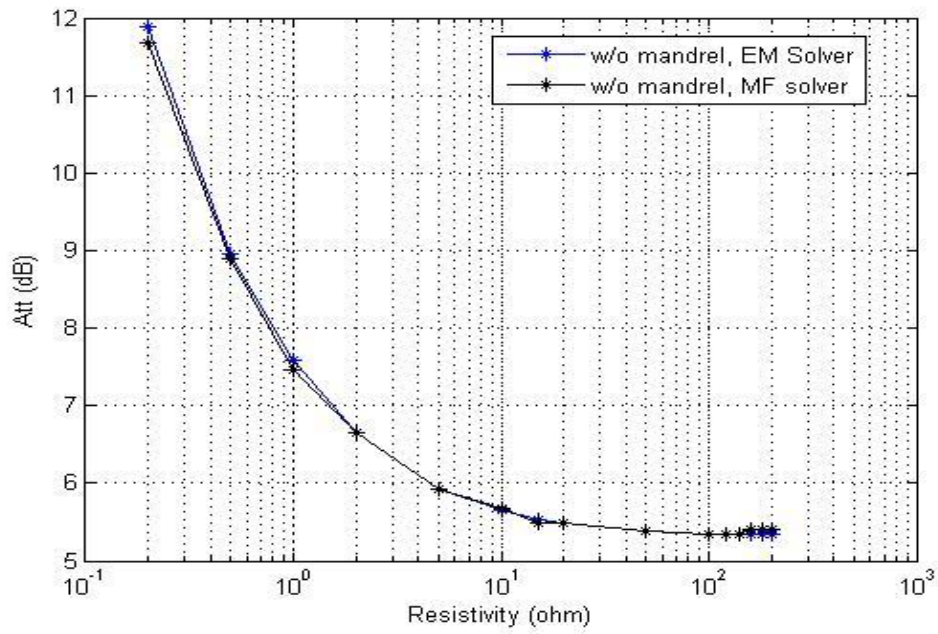


Fig. 26 Attenuation versus resistivity

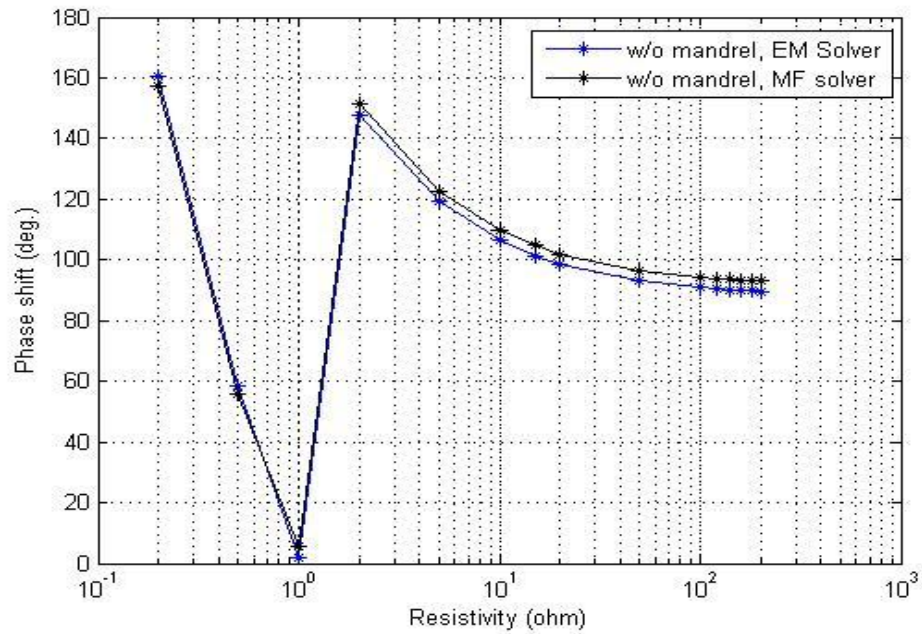


Fig. 27 Phase shift versus resistivity

3.3 EM responses of z-directed coils in a two-layer formation

The 3D model is designed with and without a mandrel respectively. This example is a case of a two-layer formation model with dipping angle of 60° . Two different materials are used in this model, they have an electrical conductivity of 0.5 S/m and 5 S/m for the top and bottom layer respectively. The depth shown in the profile formation of Fig. 28 are measured depth (MD). The bed boundary is set at zero MD.

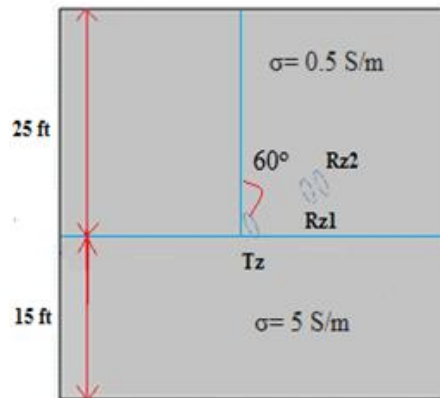


Fig. 28 Profile of a two-layer isotropic formation

Transmitter and receivers are z-directed coils with same TR spacing of 28 inches and RR spacing of 6 inches. The 3D COMSOL model for two-layer isotropic formations is shown below in Fig. 29. In this model, extra-fine mesh is used for the design portion to achieve better accuracy. The number of tetrahedral elements is found to be 413,625 with the maximum element size of 0.427 m for the case without mandrel.

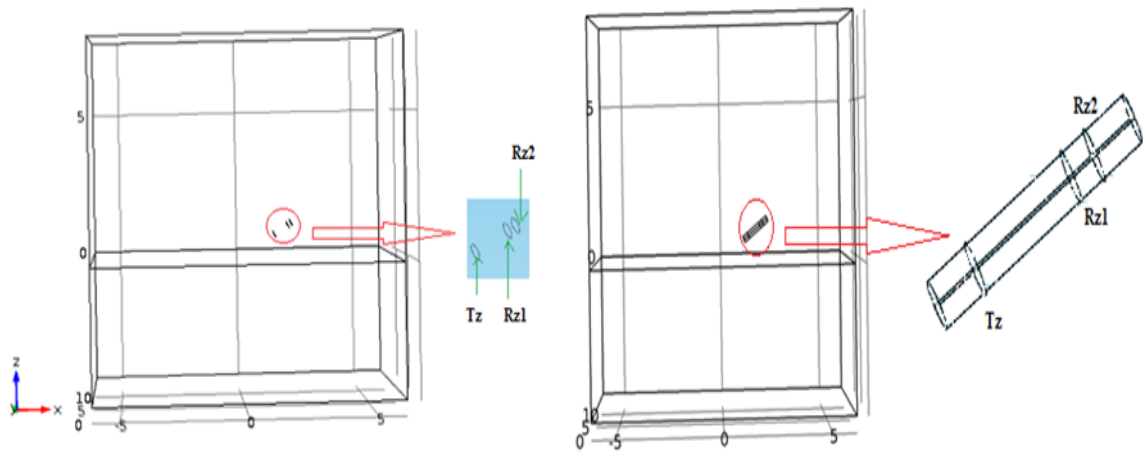


Fig. 29 3D COMSOL model (a) without a mandrel, (b) with a mandrel

For the case with a mandrel, the maximum element size value of 0.427 m and minimum element size value is 0.0183 m and the number of tetrahedral elements is 414,347 for the case with a mandrel. Fig. 30 shows the mesh structure used for EM solver without a mandrel.

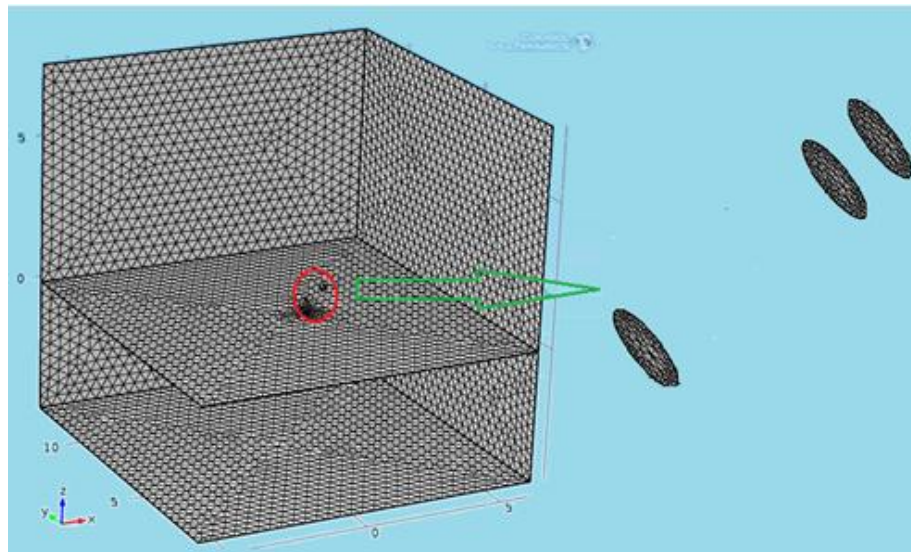


Fig. 30 Mesh structure without a mandrel

EM field is created at the tool frequency of 2 MHz and scattering boundary condition is fixed to the outer boundary. Fig. 31 and Fig. 32 show the slice view of EF distribution of z-directed coil in zx-plane using EM solver at a depth of -3 ft respectively. The EF strength is high in between -125 to -160 dB for the case with and without a mandrel, and the strength of EF becomes low beyond -160 dB.

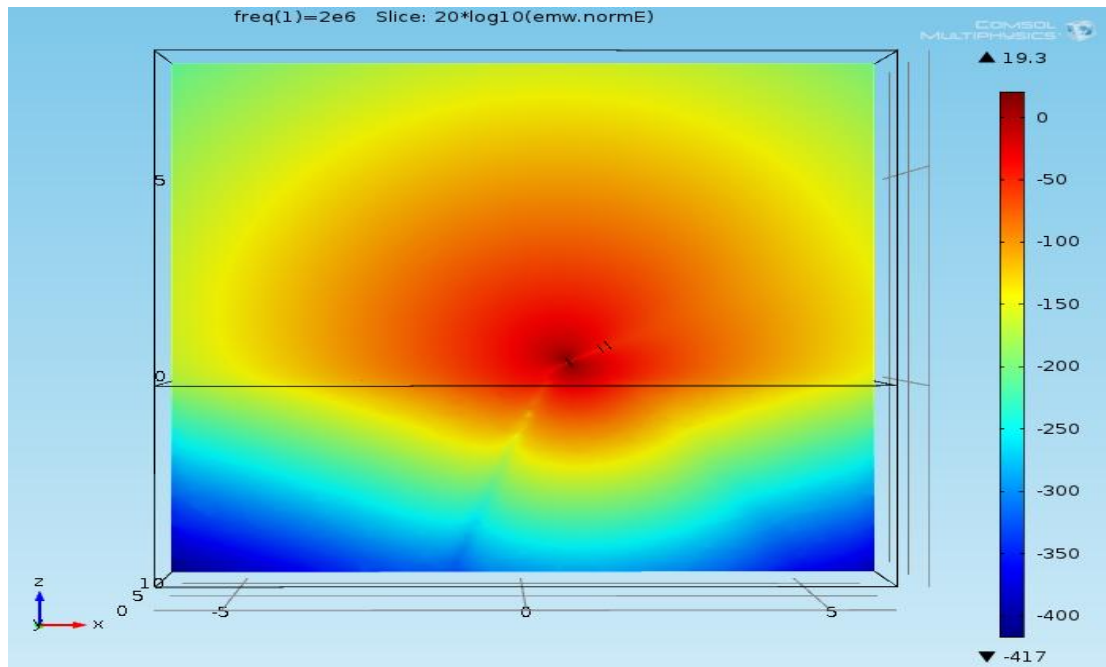


Fig. 31 EF distribution without a mandrel

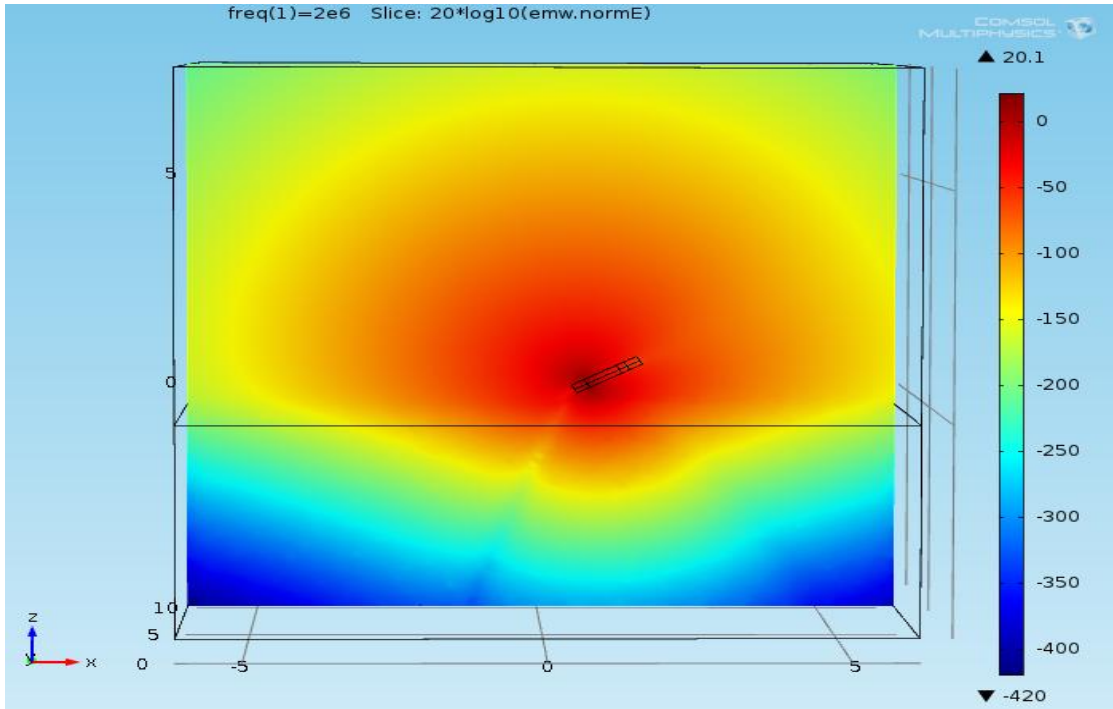


Fig. 32 EF distribution with a mandrel

Simulation is performed with the depth varying from -15 to 10 ft. The memory size utilized for the simulation is 1.45 GB with the total run time for 26 points is found to be 9,448.4 sec. The characteristic plots of attenuation and phase shift versus MD are shown in Fig. 33 and Fig. 34 respectively. Here, we can see that the response from EM solver and MF solver with and without using a mandrel looks similar on attenuation plot however for phase plot there is little deviation in the cases with and without a mandrel. The value is off by 4° from -15 to 0 ft and the plot looks similar from 1 to 4 ft and off by 4° from 5 to 10 ft.

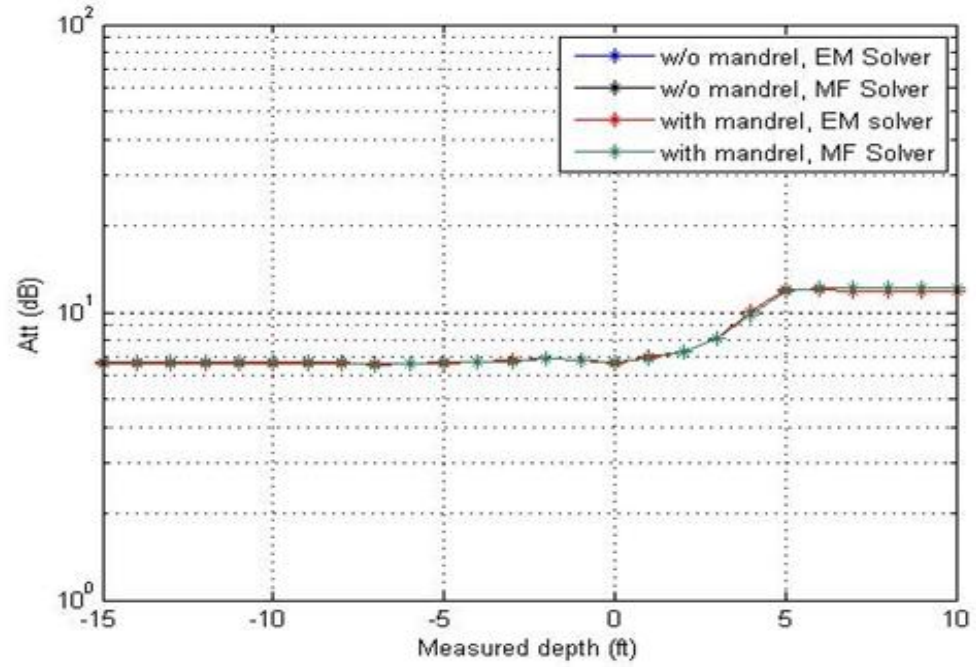


Fig. 33 Attenuation versus measured depth

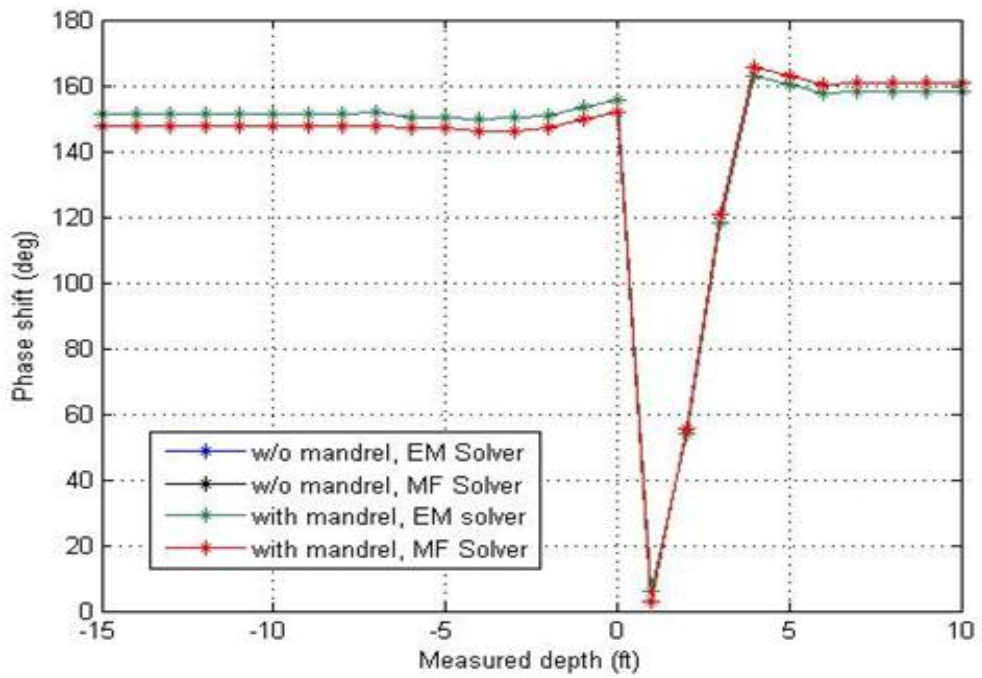


Fig. 34 Phase shift versus measured depth

3.4 EM responses of z-directed coils in a three-layer formation

Fig. 35 shows the profile formation for the case with a three-layer formation. The model is designed with and without a mandrel. Top and bottom layers have $\sigma = 1$ S/m, the middle layer, dipping layer, having $\sigma = 0.1$ S/m with $\epsilon_r = 1$ and $\mu_r = 1$. In this model, similar set up like z-directed coils in the homogenous formation are used for the transmitter, receivers and mandrel regarding the spacing, radius and height. A finite size transmitter and receiver loop antenna are used having a radius of 4.5 inches with TR spacing of 28 inches and RR spacing of 6 inches.

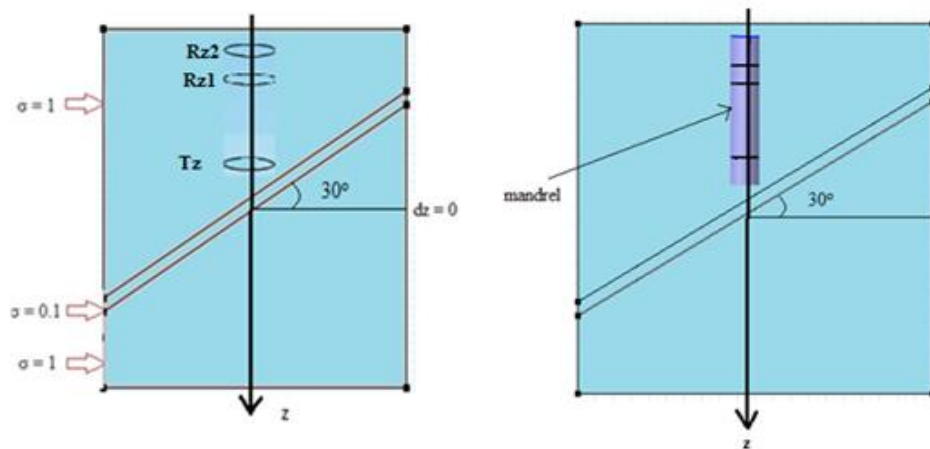


Fig. 35 Profile of a three-layer formation

In this model the scattering boundary condition is set to be the outer boundary. The cases we used is finite size antenna, they are not axis symmetrical. They are 3D COMSOL models as shown in Fig. 36, and calculations on these 3D models will be conducted using COMSOL. Three circles represent one transmitter and two receivers with the cylinder representing the metallic mandrel. The metallic mandrel used is steel

having a radius of 4 inches and height of 51 inches with $\sigma = 0.1 \text{ S/m}$, $\epsilon_r = 20$ and $\mu_r = 1200$.

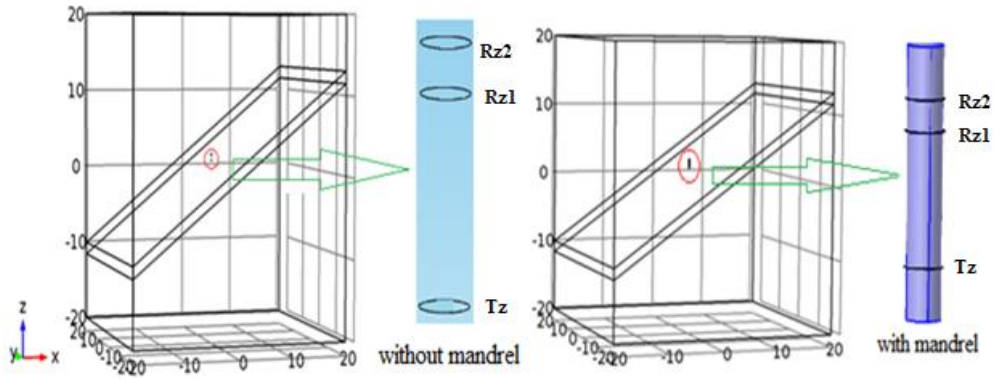


Fig. 36 3D COMSOL model

A line source ($I = 1 \text{ A}$) is assigned to the transmitter loop and complex voltages are calculated on the two receiver loops respectively to obtain attenuation and phase shift. Both transmitter and receivers are z -directed magnetic dipoles. The edge current in the transmitter is represented by blue color in the Fig. 37 and it is represented as a line source.

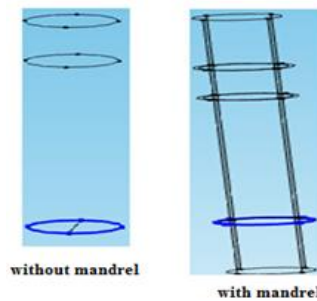


Fig. 37 Edge current in transmitter acting as source

An edge current is used to excite transmitter, transmitter and receiver are modeled as a finite size loop with an infinitesimal thin wire. Normal mesh is not giving adequate results so finer mesh is used to achieve better accuracy. With finer mesh the number of tetrahedral elements are also increased for the case without and with a mandrel, and are 110,947 and 112,128 respectively decreasing the maximum element size than the normal mesh, i.e., 2.2 m. The finer mesh leads to an increase in the number of tetrahedral elements. Fig. 38 shows the mesh structure used for the case with a mandrel using EM solver.

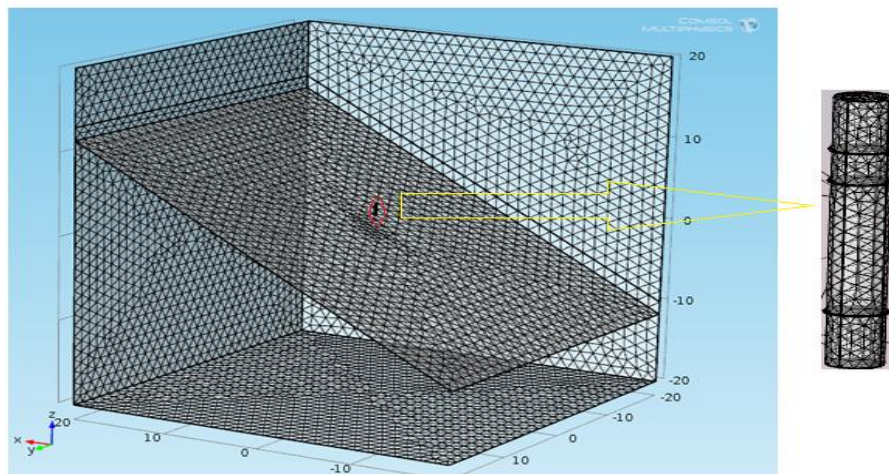


Fig. 38 Mesh structure with a mandrel

The scattering boundary condition is set to the outer boundary and EM field is created at the frequency of 2 MHz. Fig. 39 and Fig. 40 show the slice view of EF distribution of z-directed coil in yz-plane using EM solver at a depth of -80 inches.

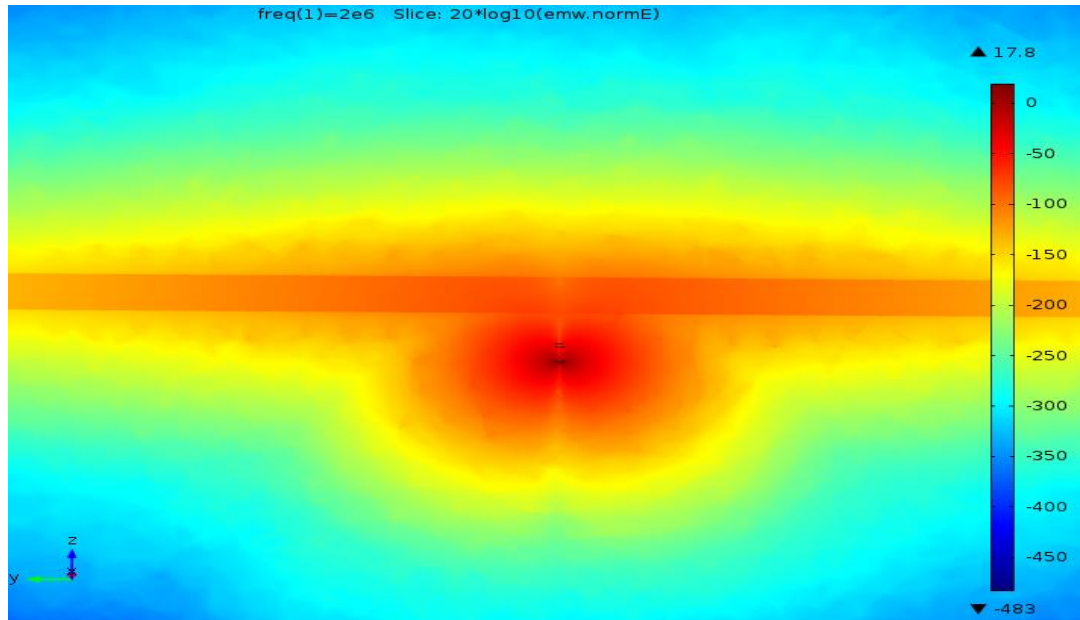


Fig. 39 Slice view of EF without a mandrel

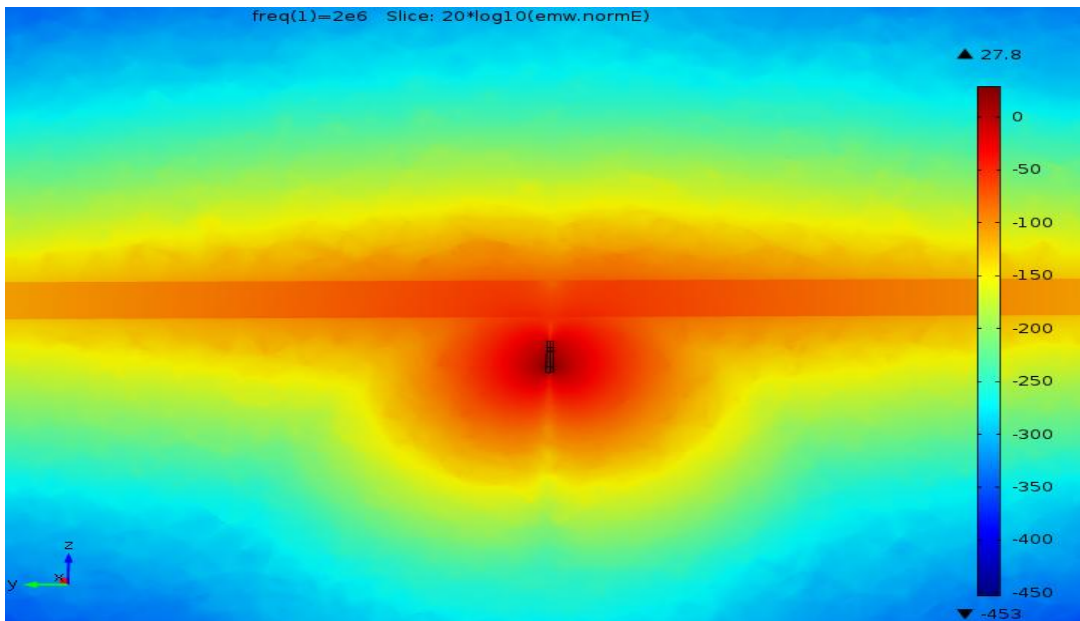


Fig. 40 Slice view of EF with a mandrel

In Fig. 39 there is a presence of strong EF between the range of -150 to -200 dB which is for the case without a mandrel and for the case with mandrel, the EF is strong between the range -125 to -175 dB as shown in Fig. 40. The simulation is performed with the depth varying from -80 to 80 inches. The memory size taken for the simulation is 1.17 GB and 1.53 GB for the case with a mandrel and without a mandrel with the total run time of 1,173 sec and 1,326 sec respectively. The tool response for attenuation and phase shift versus MD are shown in Fig. 41 and Fig. 42 respectively. In Fig. 41, we can see that results from EM solver and MF solvers are similar for the case with and without a mandrel. The presence of a mandrel produces a decrement in the attenuation values, but there is the reverse case for phase shift plot. After analyzing these plots, the presence of a mandrel produces a downward shift (~ 3 dB) in attenuation plot but has an upward shift (~ 55 deg.) on the phase shift plot.

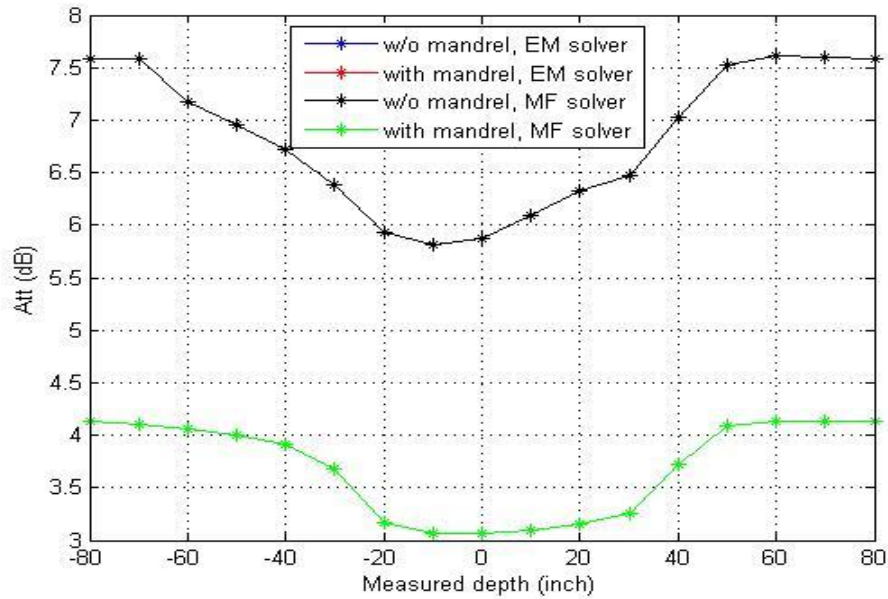


Fig. 41 Attenuation versus measured depth

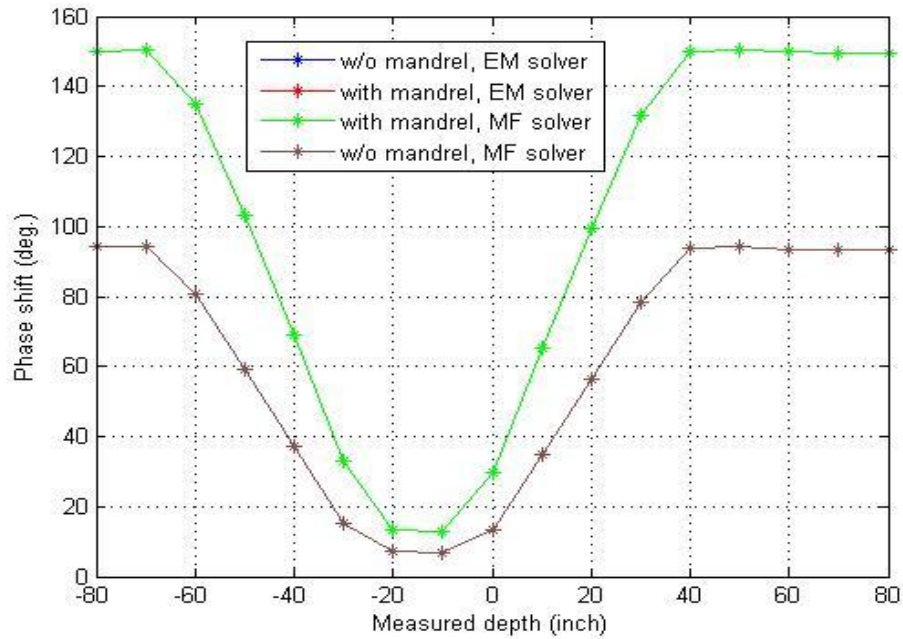


Fig. 42 Phase shift versus measured depth

3.5 EM responses of x-directed coils in layered isotropic formation

Fig. 43 shows the profile with a two-layer isotropic formation. The model is designed with and without a mandrel, top layer having $\sigma = 5$ S/m and bottom layer having $\sigma = 10$ S/m. A finite size transmitter and receiver loop antenna are used having a radius of 2.5 inches for the case without a mandrel. For the case with a mandrel, the radius size is 4.5 inches for transmitter and receiver loop antenna and the mandrel has a radius of 4 inches and height of 51 inches with $\sigma = 0.1$ S/m, $\epsilon_r = 20$ and $\mu_r = 1200$.

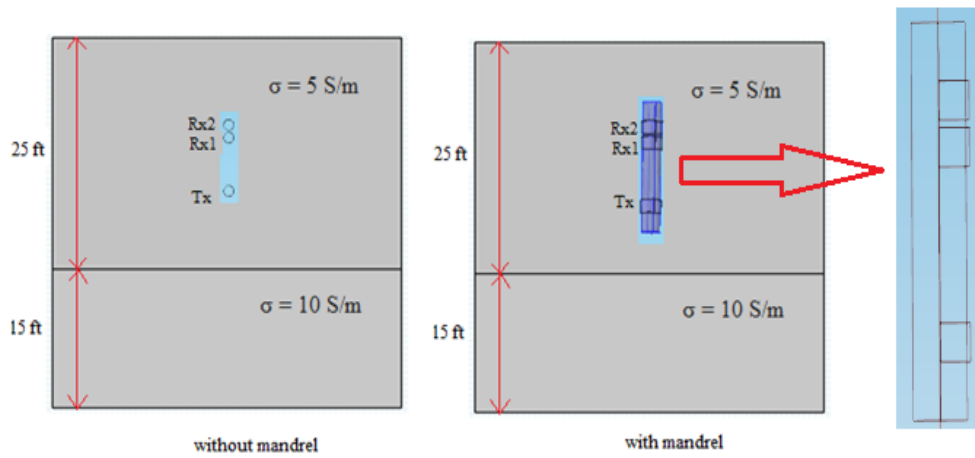


Fig. 43 Profile of a two-layer isotropic formation

The 3D model for the two-layer isotropic formation is shown below in Fig. 44 and the design uses a TR spacing of 28 inches and RR spacing of 6 inches also, both transmitter and receivers are x-directed dipoles.

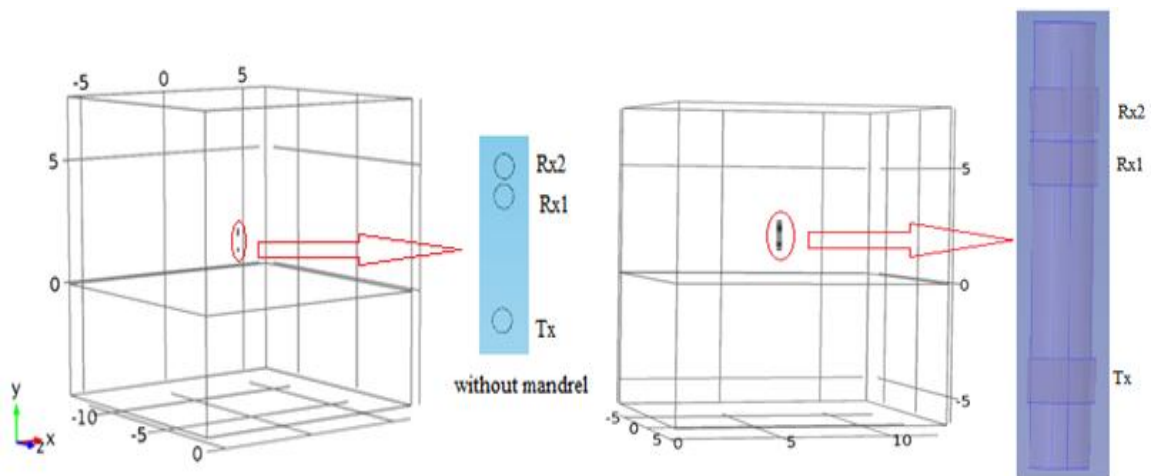


Fig. 44 3D COMSOL model (a) without a mandrel, (b) with a mandrel

To obtain the accurate results, extra-fine mesh is used and the mesh structure for this 3D model is shown in the Fig. 45, which leads the field to be smooth. The computing time is longer compared to the time of normal mesh computing. With extra-fine mesh, the number of tetrahedral elements is also increased, decreasing its maximum element size. The numbers of tetrahedral elements are 333,194 and 389,853 respectively for the cases without and with a mandrel. The maximum element size is same for both cases, i.e., 0.427 m. It is obvious that increasing the mesh size will increase the memory size.

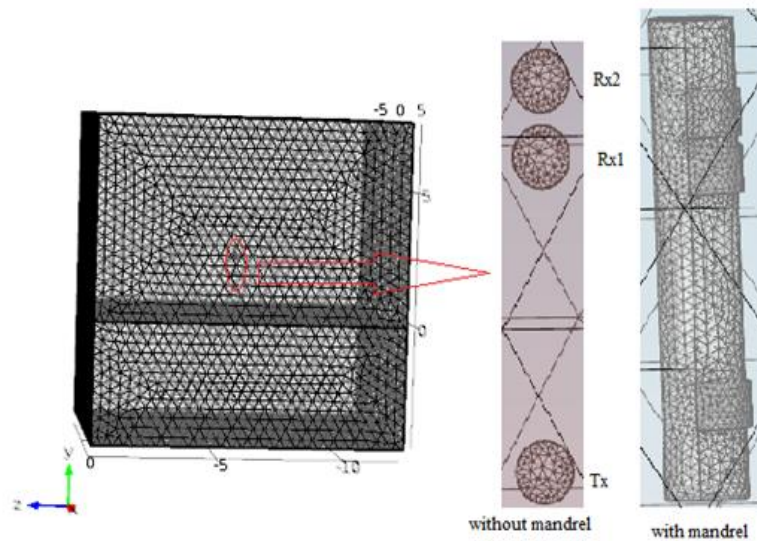


Fig. 45 Mesh structure

An EM field is created at the frequency of 2 MHz for both the cases and the scattering boundary condition is set to the outer boundary. To reduce the size of the simulation domain the impedance boundary can be applied instead of the scattering boundary at the edge of the overall domain. With a mandrel an EF is created only on the two edges of the transmitter. A transmitter antenna excites eddy current ($I = 1A$) as a line

source in its loop and complex signals are calculated on the two receiver antennae, and then convert the amplitude ratio and phase shift of these two signals to attenuation resistivity and phase shift resistivity. Fig. 46 and Fig. 47 show the slice view of an EF distribution in a transmitter and receiver that is x-directed in the xy-plane using the EM solver at a depth of -10 ft. It is shown that there is strong EF at -200 dB.

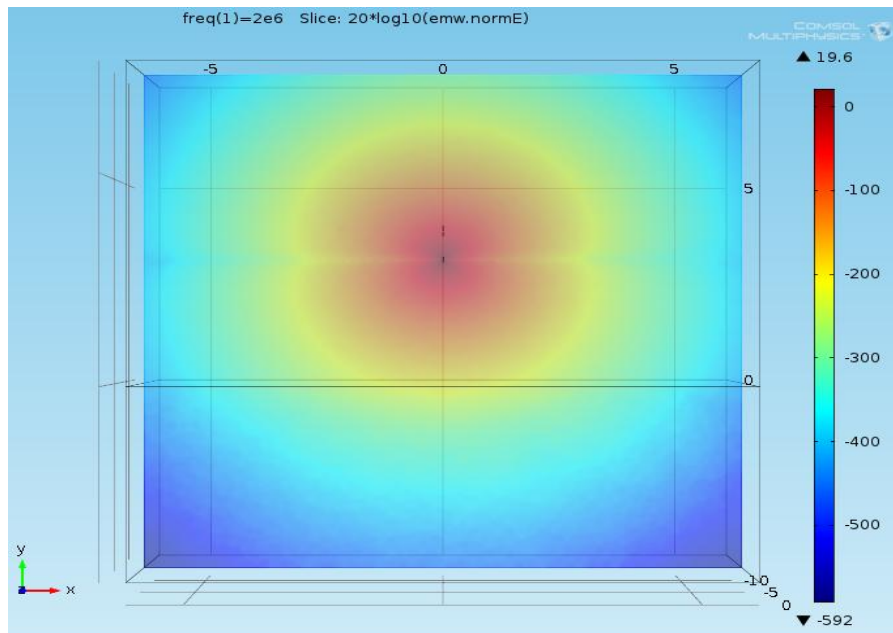


Fig. 46 Slice view of EF distribution in xy plane without a mandrel

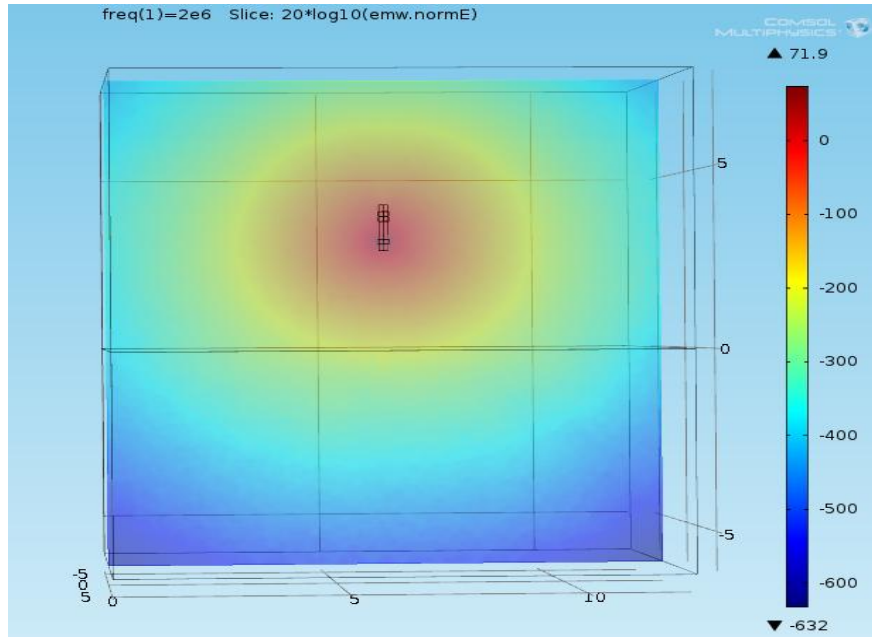


Fig. 47 Slice view of EF distribution in xy plane with a mandrel

The simulation is performed with the MD varying from -15 to 15 ft. The memory size taken for the simulation are 1.17 GB and 1.36 GB for the case with and without a mandrel with the total run time for the calculation of 31 depth points is 7,607.4 sec and 9,672 sec respectively. Fig. 48 shows the tool response for attenuation versus MD. We can see that the results of the COMSOL 3D model from the EM solver and MF solver without using a mandrel are similar to the reference result without a mandrel. Comparing these plots, at a depth of -15 ft, attenuation is found to be 10.44 dB for both the cases. For a depth of -1 ft, attenuation is 10.51 dB for the reference result and 10.44 dB for the EM solver without a mandrel. Similarly, at a depth of 1 ft, attenuations are 13.86 dB and 10.56 dB. For the depth of 2 ft, attenuations are 13.84 dB and 11.25 dB respectively. Then the values of attenuation (dB) are the same after a depth of 3 ft. This shows that the results from 3D COMSOL using the EM solver and MF solver are very close to the

reference results. Fig. 49 shows the reference resistivity versus attenuation with and without a mandrel.

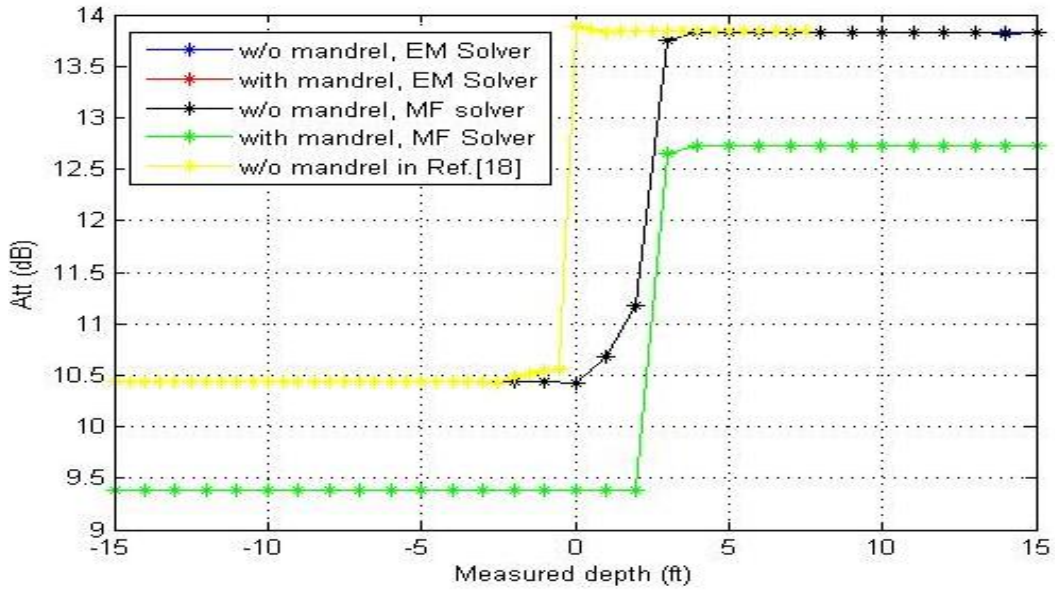


Fig. 48 Attenuation versus measured depth

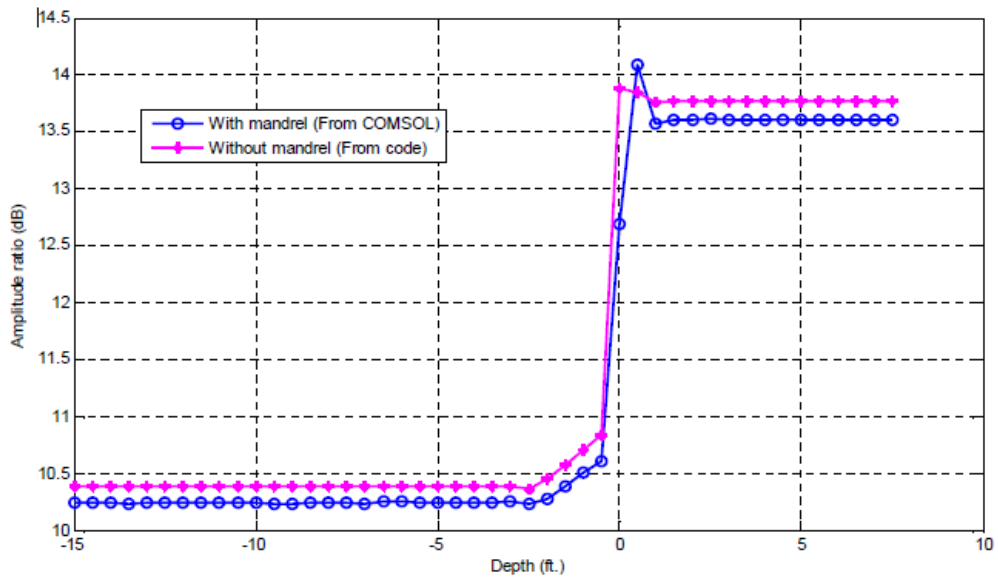


Fig. 49 Resistivity versus attenuation (from Ref. [18])

Fig. 48 shows that the presence of a mandrel produces a downward shift in attenuation (~ 1 dB). The presence of a mandrel does not produce a visible effect in the isotropic layer. Generally, the effect of a mandrel is distinguishable in a more resistive formation. Fig. 50 shows the tool response for the phase shift and there is an upward shift (~ 25 deg.) in the phase difference with the effect of a mandrel.

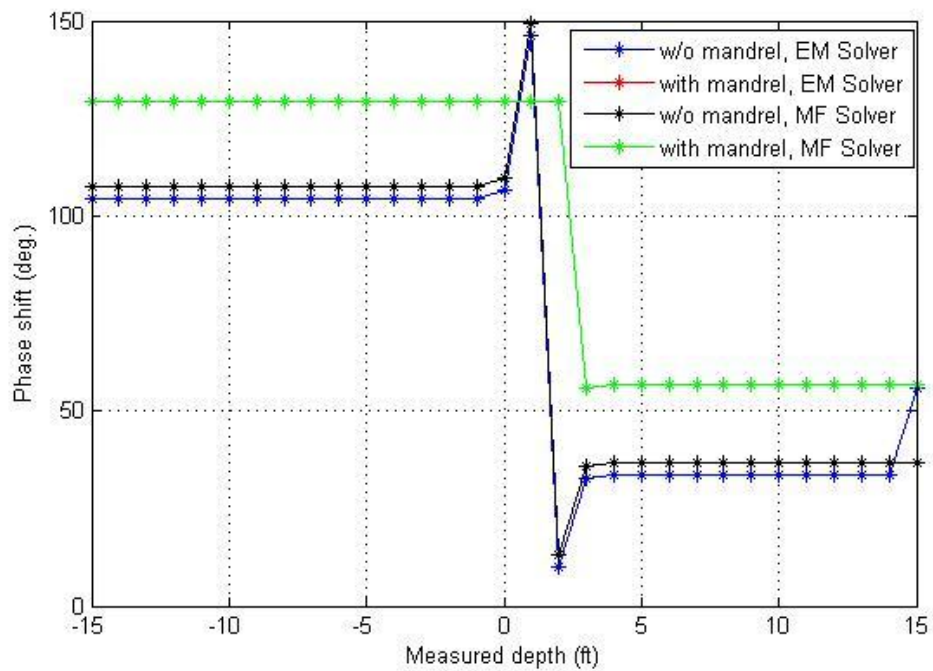


Fig. 50 Phase shift versus measured depth

Chapter 4 EM responses of dipoles in the anisotropic media

Consider Maxwell's equations in an anisotropic medium given by following equations

$$\nabla \times \mathbf{E} = -\mu \frac{\partial \mathbf{H}}{\partial t} - \mathbf{M} \quad (4.1)$$

$$\nabla \times \mathbf{H} = -\epsilon \frac{\partial \mathbf{E}}{\partial t} + \sigma \mathbf{E} + \mathbf{J} \quad (4.2)$$

where \mathbf{E} , \mathbf{H} and \mathbf{J} are the EF, MF and electric current density, respectively.

The electrical anisotropy measurement is difficult. As the development of triaxial induction, detection of anisotropy of the media becomes an important area of interest. One example of an anisotropic formation is the laminated sequences of thin layers of shale and sand formations. In this type of anisotropic formations, the horizontal conductivity is frequently regulated by shale formations but the vertical conductivity is directed by the hydrocarbon-bearing sand formations [19].

The anisotropic formation affects analysis of induction logging. The effect of anisotropy on resistivity logs depends on the angle between the borehole and formation. In the vertical wells with flat-lying beds, the current flows parallel to bedding and an induction tool measures only the horizontal resistivity. Then the notion of a single number for true resistivity (R_t) can be used to interpret the tool responses. With increasing well deviations, the contribution from the vertical resistivity becomes stronger. Therefore, the use of true resistivity (R_t) becomes less useful as electrical anisotropy increases. Two resistivities, the vertical resistivity (R_v) and horizontal resistivity (R_h), are more precise to describe the formation anisotropy. In horizontal wells through flat-lying beds, resistivity logs read higher because the contribution of vertical resistivity reaches a maximum.

EM induction logging tools are susceptible to the electrical conductivity of earth formations. These electrical conductivities tend to be anisotropic because of geological impacts such as the presence of the amount of mud and sand which laminates with directional conductivities. During vertical drilling, earth formation conductivity is represented as 3×3 diagonal matrix, i.e., diagonal tensor in a Cartesian co-ordinate system given by

$$\sigma = \begin{bmatrix} \sigma_h & 0 & 0 \\ 0 & \sigma_h & 0 \\ 0 & 0 & \sigma_v \end{bmatrix} \quad (4.3)$$

where σ_h is horizontal conductivity and σ_v is vertical conductivity [20]. The anisotropy ratio is defined by the term k , as follows

$$k = \left(\frac{\sigma_h}{\sigma_v}\right)^2 \quad (4.4)$$

If the principal anisotropy and logging tool axes do not coincide with each other, the electrical conductivity tensor is represented by a full 3×3 tensor.

4.1 EM responses of x-directed coils in a single-layer formation

Fig. 51 shows the profile formation of a single-layer homogeneous anisotropic medium. The 3D model is designed without a mandrel, and a finite size transmitter and receiver loop antenna is used having a radius of 2.5 inches and the material used for the block having following property as $\epsilon_r = 1$ and $\mu_r = 1$. The 3D COMSOL model for the single-layer anisotropic formation is shown in the Fig. 52 with TR spacing of 28 inches and RR spacing of 6 inches. Both the transmitter and receivers used for the design of induction tool are x-directed dipoles.

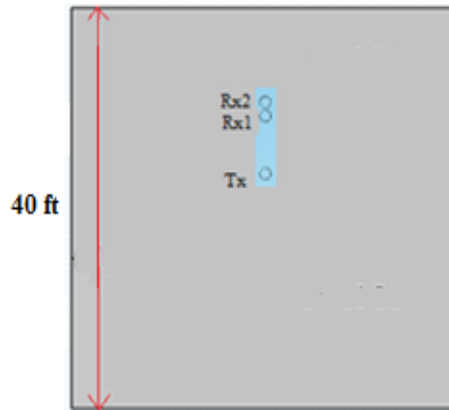


Fig. 51 Profile of a single-layer anisotropic formation

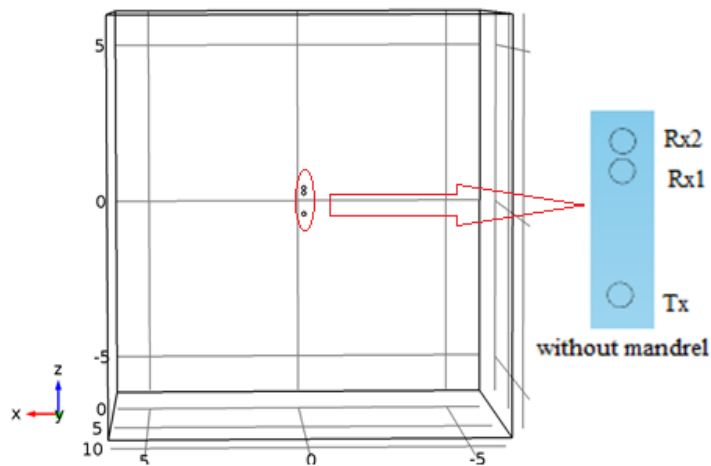


Fig. 52 3D COMSOL model without a mandrel

A line source of 1A current is assigned to the transmitter loop and complex voltages are measured on the two receivers. Extra fine mesh is used in this case with the number of tetrahedral elements to be 424,979 and the maximum element size to be 0.427 m. The scattering boundary condition is set to the outer boundary and an EM field is created at the operating frequency of 2 MHz.

Fig. 53 shows the mesh structure used for the EM solver without a mandrel for the design. The simulation is performed keeping horizontal conductivity constant, i.e., $\sigma_h = 1$ S/m and varying vertical conductivity (σ_v) from 0.005 to 5 S/m. Fig. 54 shows the slice view of an EF distribution without a mandrel using the EM solver at $\sigma = 0.005$ S/m.

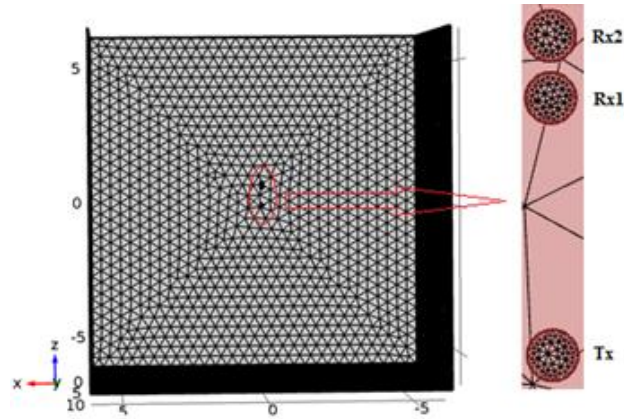


Fig. 53 Mesh Structure

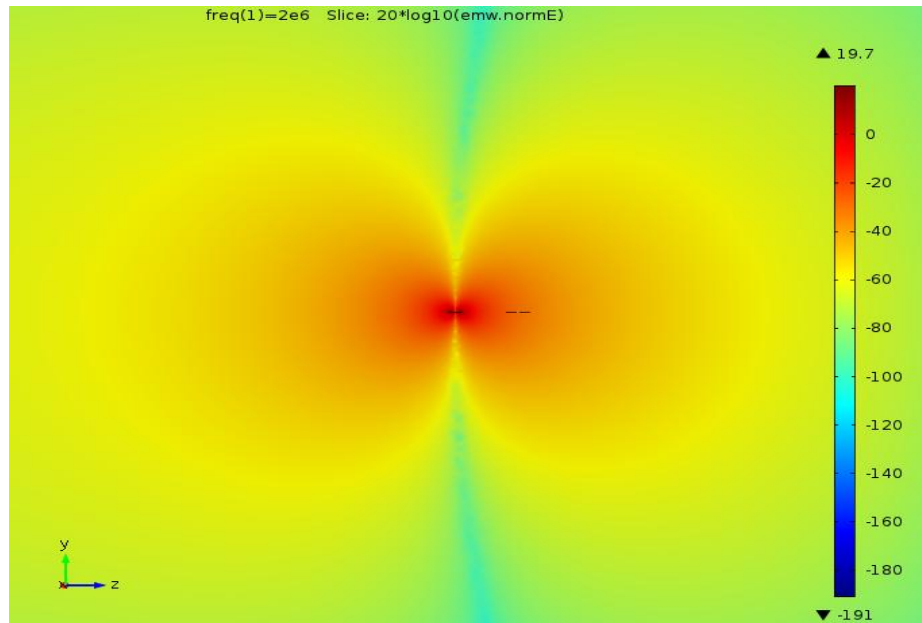


Fig. 54 Slice view of EF distribution without a mandrel

The characteristic plots of attenuation and phase shift versus resistivity is plotted using the EM solver and MF solver are shown in the Fig. 55 and Fig. 56. Also, attenuation and phase shift plots are similar for both the EM and MF solvers. In Fig. 55, attenuation increases as there is an increment in resistivity, at the resistivity of 0.2 Ω , attenuation is 5.725 dB. As the resistivity progresses, attenuation increases linearly for both the EM and MF solver. The attenuation is constant, i.e., 6.65 dB for the two solvers from the resistivity of 5 Ω . Also, this is true for phase shift versus resistivity plot in Fig. 56, phase shift is 45.5° for both solvers and increases linearly along with the increase of resistivity. Also, phase shift is constant of 62.5° at the resistivity of 100 Ω .

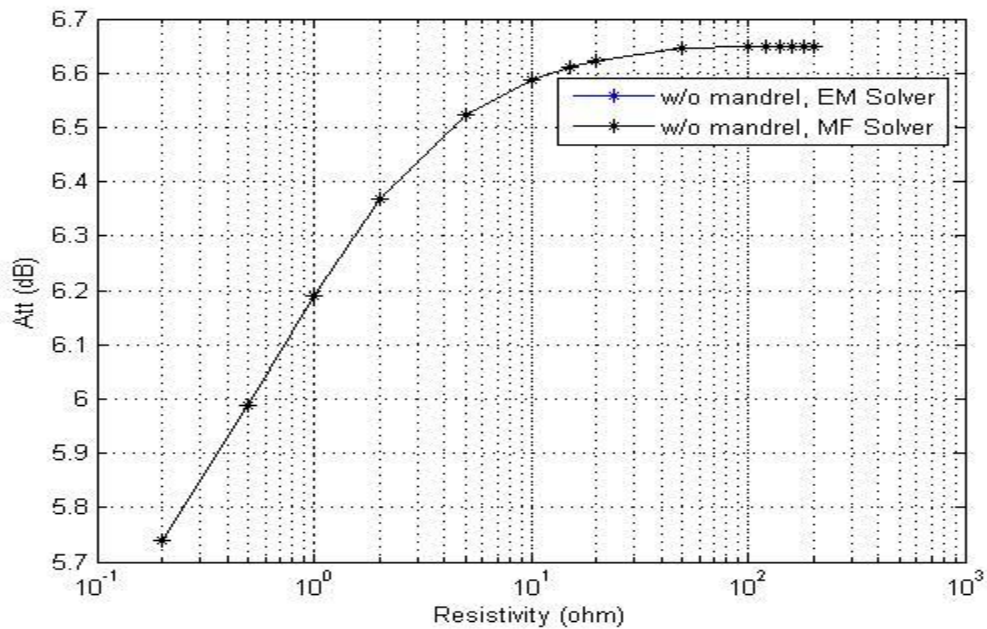


Fig. 55 Attenuation versus resistivity

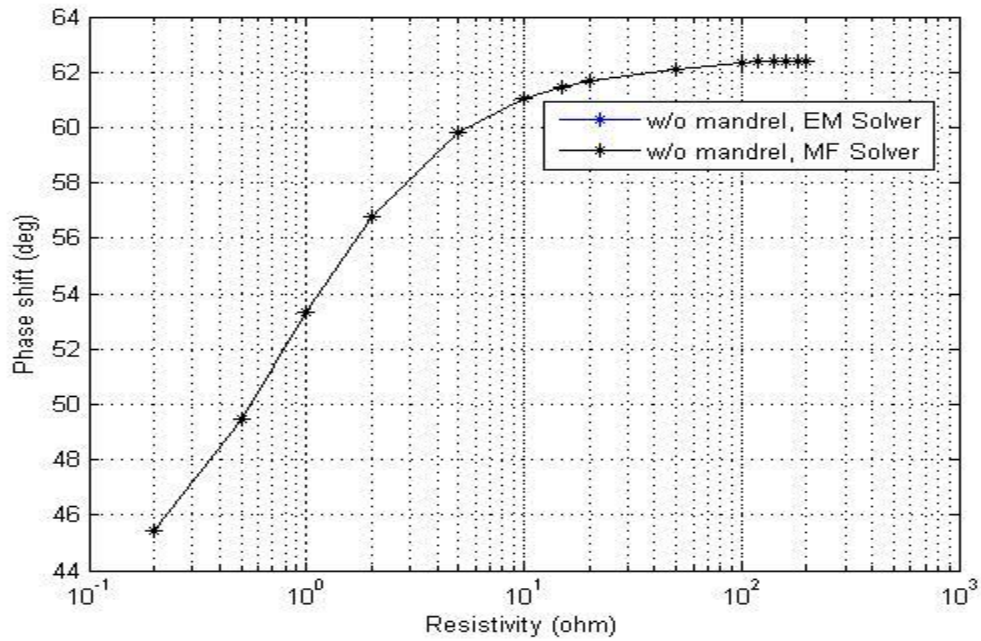


Fig. 56 Phase shift versus resistivity

4.2 EM responses of z-directed coils in the anisotropic layered beds

The setup is similar to isotropic beds with z-directed coils for the case with and without a mandrel. But in the anisotropic case for both layers, the horizontal direction conductivity (σ_h) is 1 S/m whereas vertical direction conductivity (σ_v) is 0.1 S/m and 0.5 S/m respectively for top layer and bottom layer. TR spacing and RR spacing are also the same for this case with the same radii size transmitter and receivers including same height and radius for the case with a mandrel. Fig. 57 shows profile formation of a two-layer anisotropic beds. The 3D COMSOL model used for the two-layer anisotropic formation without and with a mandrel looks similar to the isotropic layered beds.

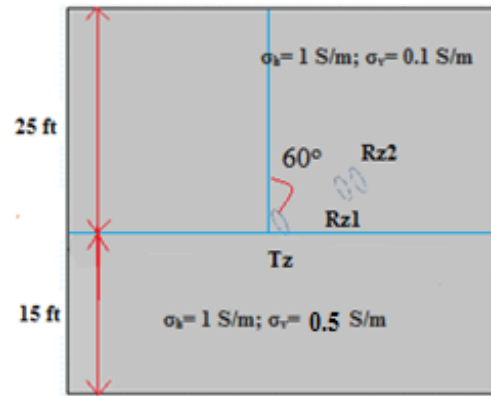


Fig. 57 Profile of a two-layer anisotropic formation

Extra-fine mesh is used in this case with the number of tetrahedral elements to be 413,625 and the maximum element size is 0.427 m. Fig. 58 shows the mesh structure used for EM solver without a mandrel for the design.

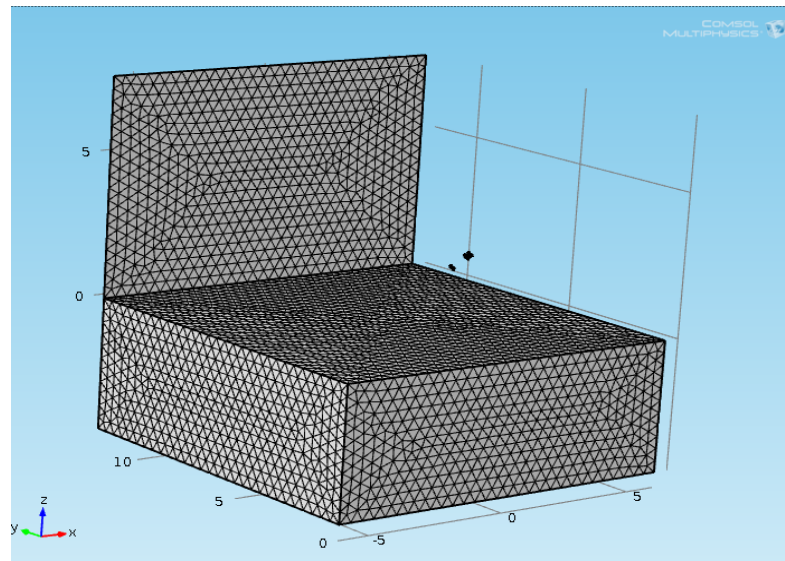


Fig. 58 Mesh structure without a mandrel

EM field is created at the frequency of 2 MHz and the scattering boundary condition is set to the outer boundary. The simulation is performed with the MD varying from -15 to 15 ft. The memory size utilized for the simulation is 1.46 GB with the run time of 10,360.2 sec for 31 depth points. Fig. 59 and Fig. 60 show the slice view of an EF distribution that is z-directed in the zx -plane using the EM solver at a depth of -3 ft. Here, the EF strength is high in between the range of -75 dB to -100 dB for the case without and with a mandrel using the EM solver. Beyond this region, the EF strength is less.

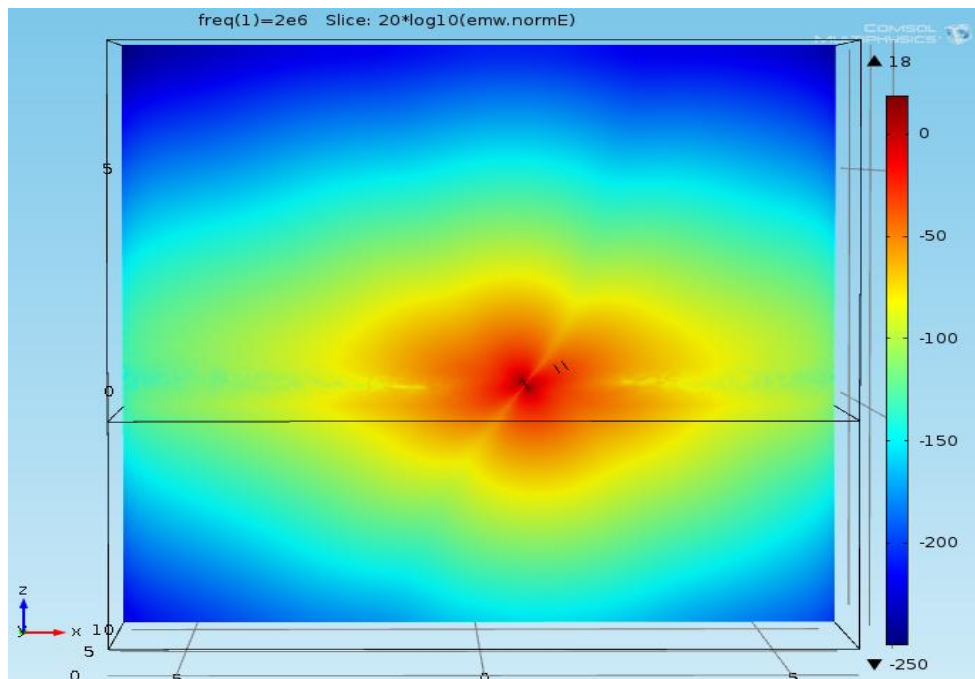


Fig. 59 EF distribution without a mandrel

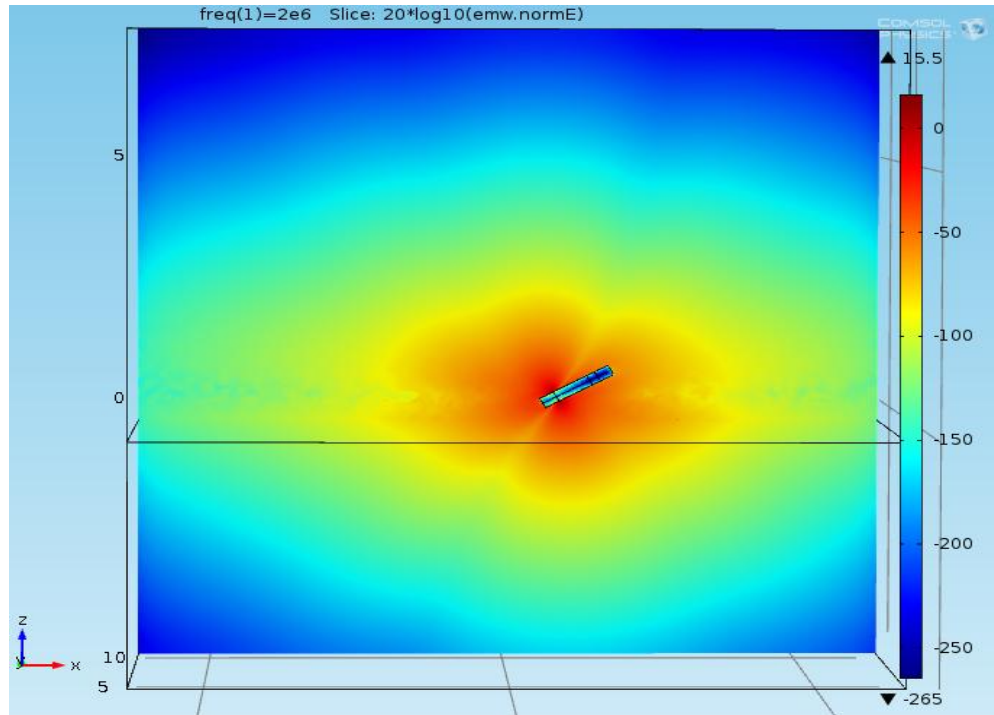


Fig. 60 EF distribution with a mandrel

Fig. 61 shows the characteristic plots of attenuation versus MD. Here, it can be seen that the response from the EM solver and MF solver, with and without a mandrel, looks similar to the attenuation plot. The value of attenuation is off for the range -1 to 1 ft. Besides this range, the attenuation values are the same. Fig. 62 shows the tool response for phase shift. The phase shift response from the EM solver and MF solver with and without a mandrel is off by 2° from -15 ft to -1 ft. The phase shift value is the same for the range 0 to 2 ft and the graph is off by 2° from 4 ft to 15 ft.

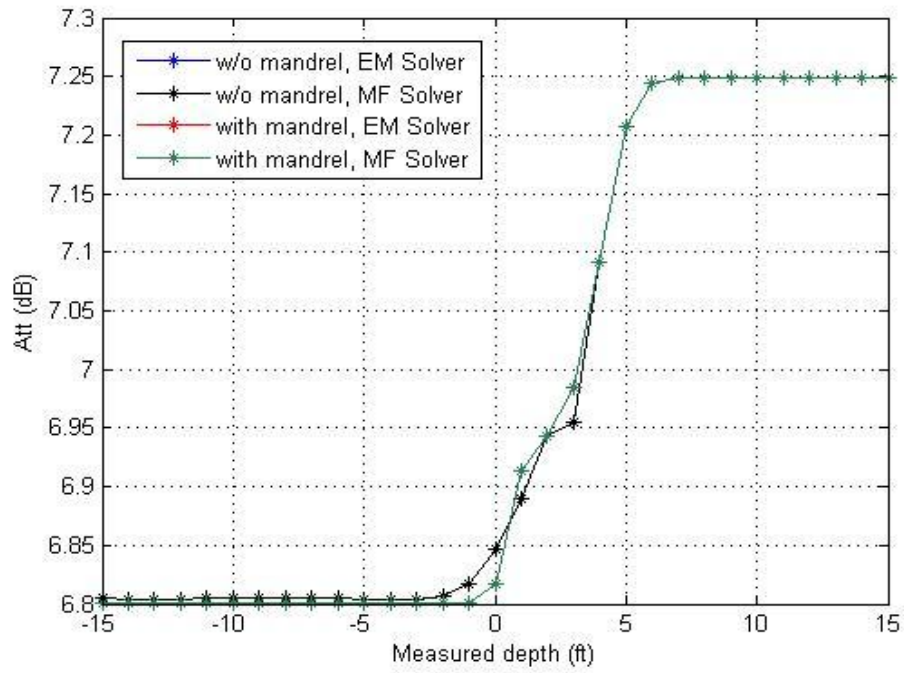


Fig. 61 Attenuation versus measured depth

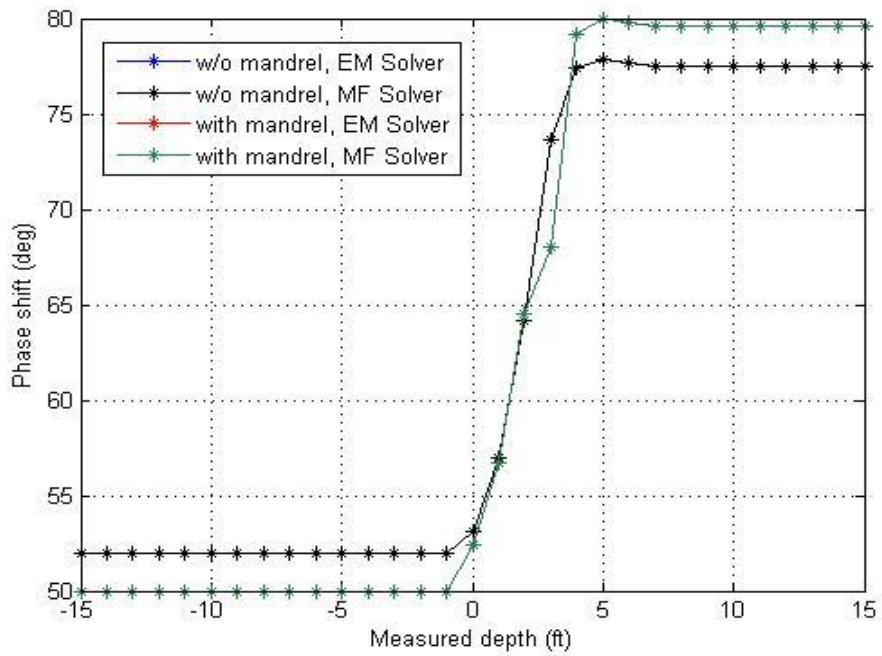


Fig. 62 Phase shift versus measured depth

4.3 EM responses of x-directed coils in the anisotropic formation:

Fig. 63 shows the profile of a two-layer anisotropic formation. The 3D model is designed with two layer, top layer with $\sigma_h=1$ S/m and $\sigma_v=0.2$ S/m and bottom layer with $\sigma_h=1$ S/m and $\sigma_v=0.1$ S/m with and without using a mandrel. The transmitter and receiver loop have the same radii size as an isotropic one with same TR and RR spacing. In this model, the transmitter and receivers are x-directed. The 3D models with and without a mandrel are the same as the isotropic formations case. The simulation is performed for both cases without and with a mandrel using the EM and MF solver. An EM field is created at the operating frequency of 2 MHz for both of these cases and the scattering boundary condition is assign to the outer boundary. Similar to the previous case of isotropic beds, with a mandrel, an EF is created only on the two edges of the transmitter. Fig. 64 and Fig. 65 show the slice view of an EF distribution using EM solver at a depth of -1 ft from the x-directed transmitter without and with a mandrel using COMSOL.

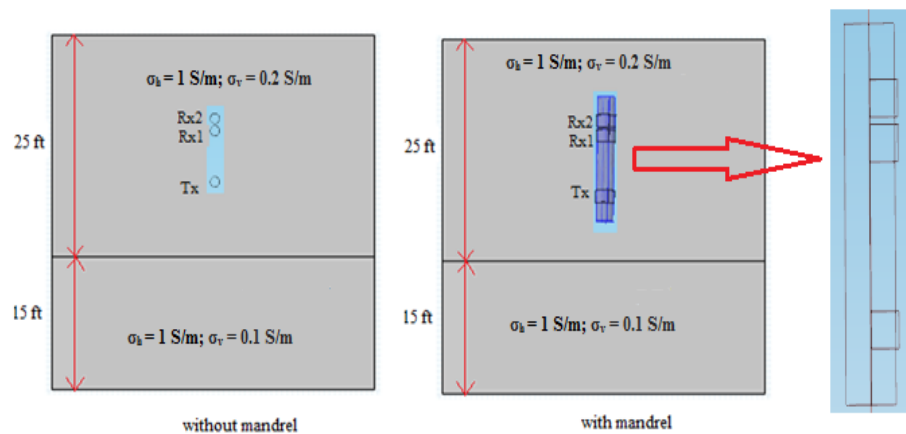


Fig. 63 Profile of a two-layer anisotropic formation

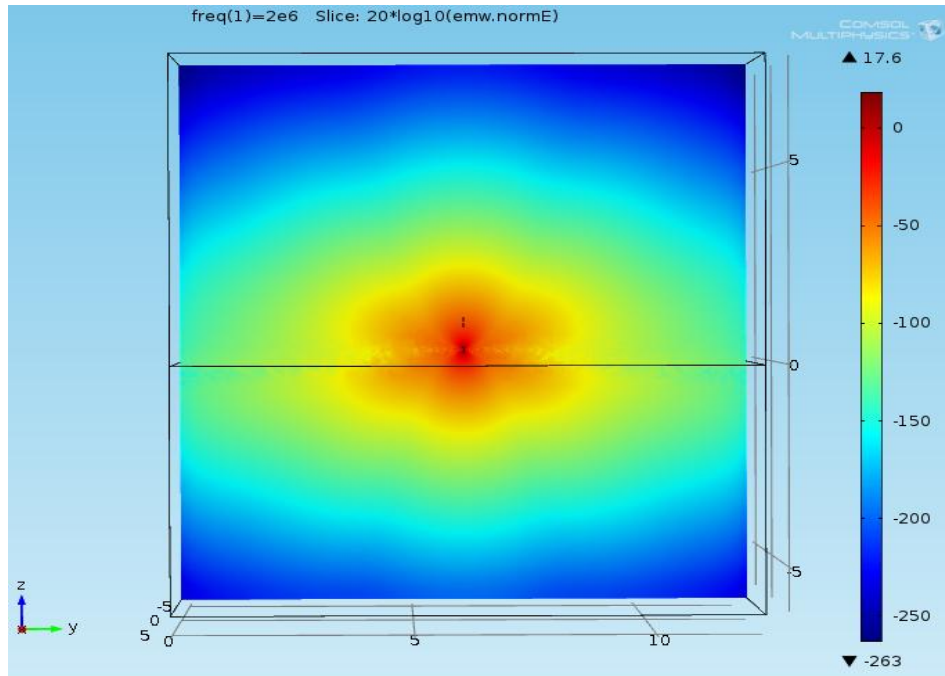


Fig. 64 EF distribution in yz plane without a mandrel

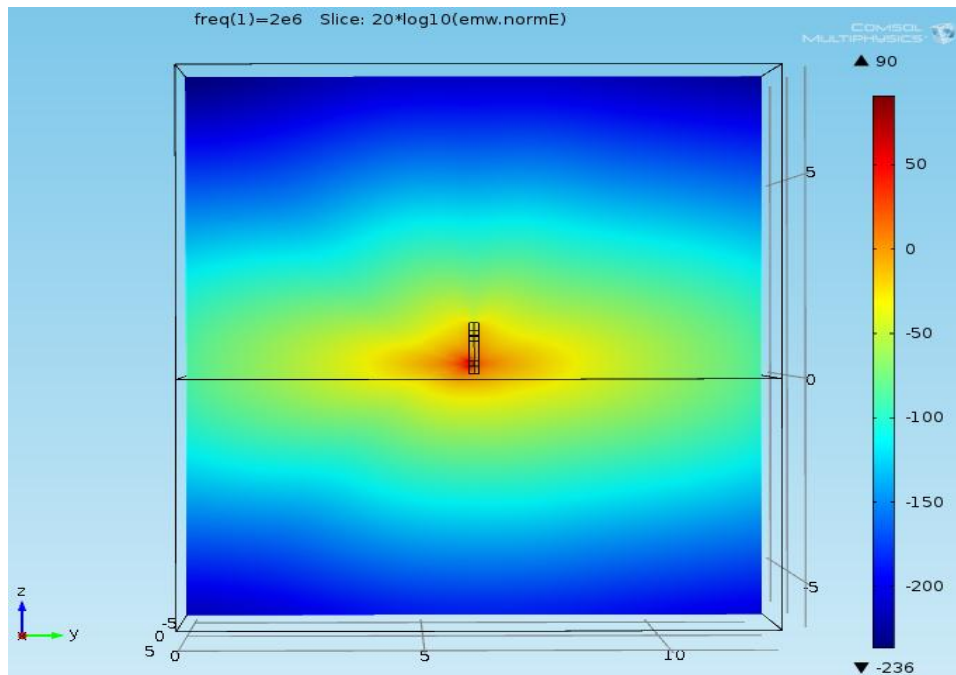


Fig. 65 EF distribution in yz plane with a mandrel

In Fig. 64 which is the case without a mandrel, the EF strength is high at -75 dB to -100 dB whereas it differs for the case with a mandrel. The EF distribution is high at -25 dB to -50 dB as seen in Fig. 65. Extra-fine mesh is used for the simulation and Fig. 66 shows the mesh structure without a mandrel. The number of tetrahedral elements are 333,194 and 389,853 respectively for the cases with and without a mandrel which turned out to be similar to the previous case. The maximum element sizes are the same for both cases, i.e., 0.48 m. Simulation is performed with the MD varying from -15 to 10 ft. The memory size taken for the simulations are 1.25 GB and 1.28 GB for the case with a mandrel and without a mandrel with the total run time for 26 depth points of 6,458.4 sec and 8,236.8 sec.

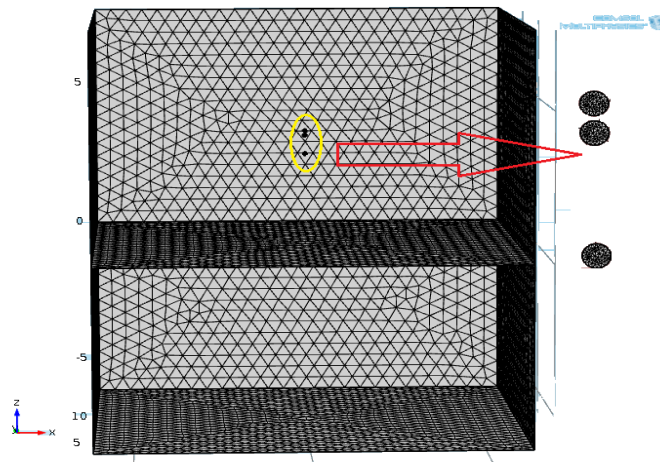


Fig. 66 Mesh structure

The tool response for attenuation versus MD is shown in the Fig. 67 and the reference result is also plotted in the same graph. Also it can be seen that the results from the COMSOL 3D model and results from the reference value are similar. Comparing

these plots, at the depth of -15 ft attenuation is 6.5 dB from COMSOL 3D for the EM and MF solvers without using a mandrel and 6.44 dB for reference. Similarly, at a depth of -5 ft, attenuations are 6.5 dB and 6.44 dB respectively. At a depth of -2 ft, attenuations are 6.5 dB and 6.48 dB. The attenuation is -6.5 dB from -1 to 2 ft for both the reference and COMSOL 3D models. The value of the reference result and COMSOL 3D models varies by 0.1 dB value which is similar. Fig. 68 shows the plot of attenuation versus MD for the reference result.

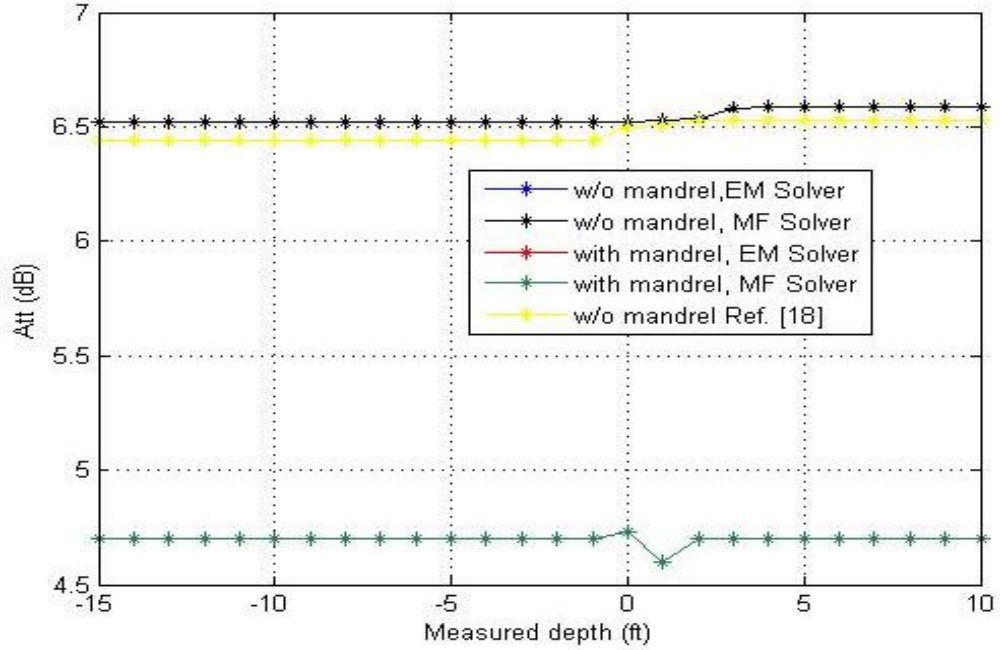


Fig. 67 Attenuation versus measured depth

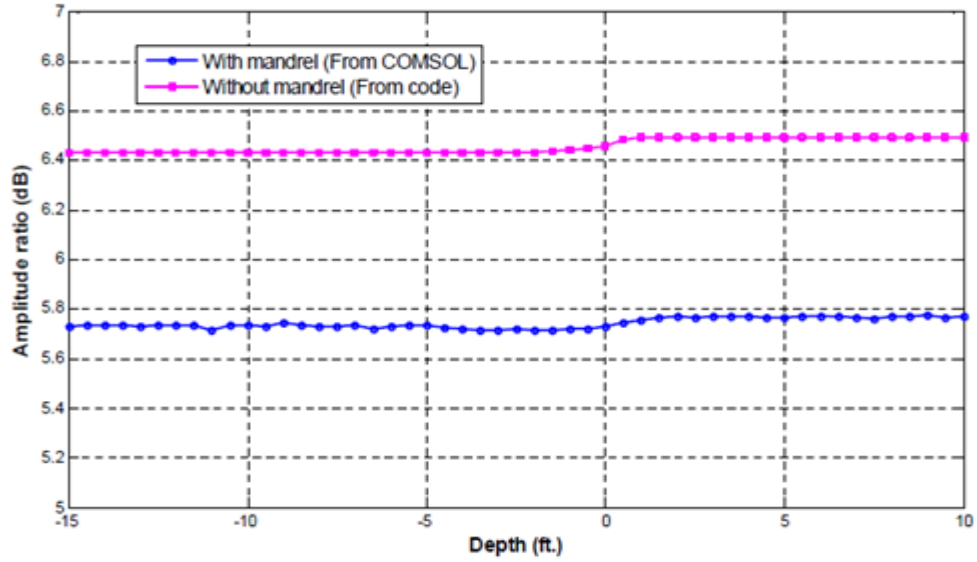


Fig. 68 Attenuation versus depth (from Ref. [18])

Fig. 69 shows the tool response for the phase shift. By looking onto these figures, the presence of a mandrel produces a significant downward shift in attenuation as well as phase shift.

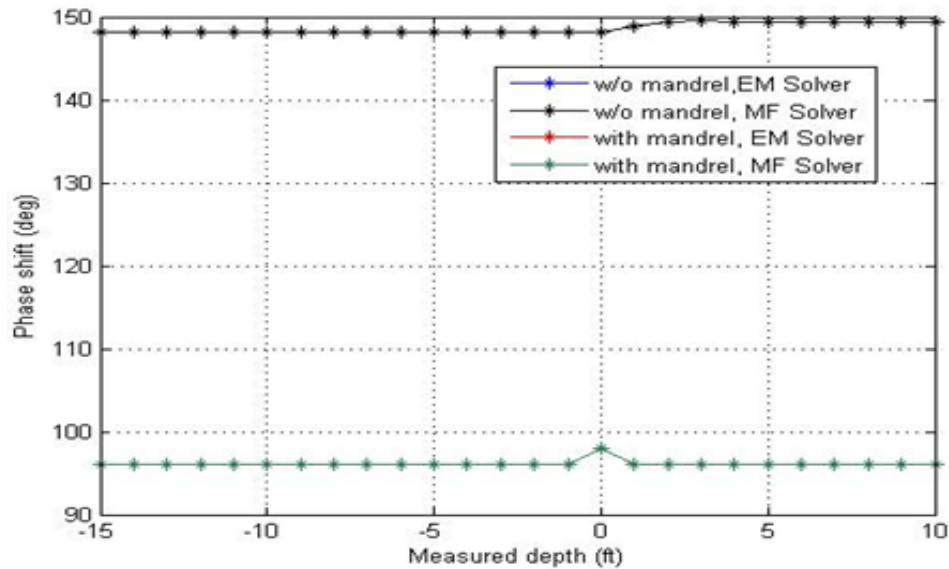


Fig. 69 Phase shift versus measured depth

Chapter 5 Conclusion and future work

5.1 Conclusion

Induction logging tools are widely used in oil and gas industry as sensor devices to measure the formation conductivity. These devices calculate the EM field strength at the receiver coils and then determine the conductivity of the surrounding formations. In the practical aspect, z-directed and x-directed coils are used to detect the earth formation and anisotropy.

In this work, EM responses of antenna coils in different formations with and without a mandrel are explored, and the amplitude ratio and phase shift are calculated for different formations. The theory of induction logging tool is briefly explained and the simulation of a newly developed induction logging tool, which contains three mutually perpendicular coils, i.e., one transmitter and two receivers, has been carried out. The 3D models are designed using COMSOL Multiphysics for the representation of an EM field. Transmitter is created as a source by supplying 1A current which creates EM field around the receivers, and the complex voltages are obtained at respective receivers using line integration. MATLAB is utilized for the calculation of attenuation and phase shifts from the value of complex voltages of the different layered formations. These 3D models consist of complex formations such as a one-, two-, and three-layers to study the EM responses.

The examples used in this thesis are illustrated to obtain the EM responses of an LWD tool operating at 2 MHz in different layered earth formations. The main idea is to investigate the effect of conductivity and MD for obtaining the EF distribution among single-, and multiple-layered isotropic and anisotropic mediums. Also, the results

obtained from EM solver and MF solver are compared for both cases with and without using a mandrel.

5.2 Future work

In the future, more results of the combination of z-directed and x-directed coils can be presented in complex form to investigate EM field. Also, with the knowledge of COMSOL software, modeling of induction logging tools, and observation of more 3D models can be further explored and presented.

References

- [1] F. T. Ulaby, E. Michielssen and U. Ravaioli, “Fundamentals of Applied Electromagnetics. Pearson,” Sixth ed., 2010.
- [2] WHO Regional Office, “Electromagnetic Fields,” 1990. [Online]. Available: <http://www.who.int/peh-emf/about/WhatisEMF/en/>. [Accessed 15 Sep 2014]
- [3] SCENIHR, “Electromagnetic Fields,” 2009. [Online]. Available: http://ec.europa.eu/health/scientific_committees/opinions_layman/en/electromagnetic-fields/1-2/1-electromagnetic-fields.htm. [Accessed 18 Sep 2014]
- [4] H. G. Doll, “Introduction to Induction Logging and Application to Logging of Wells Drilled with Oil Base Mud,” *Petroleum Technology*, vol. 1, June 1949.
- [5] L. Zhong, J. Li, L.C. Shen and R. C. Liu, “Computation of Triaxial Induction Logging Tools in Layered Anisotropic Dipping Formations,” *IEEE Transactions on Geoscience and Remote Sensing*, vol. 46, no. 4, April 2008.
- [6] H. O. Lee, “Numerical Modeling of Electromagnetic Well-Logging Sensors,” Ohio State University, 2010.
- [7] Y. K. Hue, “Analysis of Electromagnetic Well-Logging Tools,” Ohio State University, 2006.
- [8] B. Anderson, T. Barber, R. Leveridge, R. Bastia, K. R. Saxena, A. K. Tyagi, J. B. Clavaud, B. Coffin, M. Das, R. Hayden, T. Klimentos, C. C. Minh and S. Williams, “Triaxial Induction – A New Angle,” Cambridge, Massachusetts, 2008.
- [9] S. Davydycheva and M. A. Frenkel, “Review of 3D Modeling and Interpretation Methods for Triaxial Induction and Propagation Resistivity Well Logging Tools,” *PIERS Proceedings*, Cambridge, July 2010.
- [10] SIAM, “COMSOL,” May 2005. [Online]. Available: <http://www.siam.org/news/news.php?id=54>. [Accessed 15 Oct 2014]
- [11] COMSOL Multiphysics, “Reference Guide,” Nov 2012. [Online]. Available: <http://nf.nci.org.au/facilities/software/COMSOL/4.3a/doc/pdf/mpH/COMSOLMulti physicsReferenceGuide.pdf>. [Accessed 28 Oct 2014]

- [12] D. D. Grieg and H. F. Engelmann, "Microstrip-A New Transmission Technique for the Klilomegacycle Range," Proceedings of the IRE, vol. 40, no. 12, pp. 1644-1650, December 1952.
- [13] Microwaves101, "S-parameters," 2014. [Online]. Available: <http://www.microwaves101.com>. [Accessed 3 Nov 2014]
- [14] W. Frei, "COMSOL Blog," Sep 2013. [Online]. Available: <http://www.comsol.com/blogs/computational-electromagnetics-modeling-which-module-to-use/>. [Accessed 10 Nov 2014]
- [15] COMSOL, "RF Module User Guide," May 2012. [Online]. Available: <https://is.muni.cz/el/1431/podzim2013/F7061/um/RFModuleUsersGuide.pdf>. [Accessed 15 Nov 2014]
- [16] Y. L. L. Coz and R. B. Iverson, "A Stochastic Algorithm for High Speed Capacitance Extraction in Integrated Circuits," Solid State Electronics, vol. 35, no. 7, pp. 1005-1012, 1992.
- [17] J. Hoffmann, C. Hafner, P. Leidenberger, J. Hesselbarth and S. Burger, "Comparison of electromagnetic field solvers for the 3D analysis of plasmonic nano antennas," Laboratory for Electromagnetic Fields and Microwave Electronics, vol. 7390, pp. 73900J-73900J-11, 2011.
- [18] Y. Kong, Q. Li and R. Liu, "Simulation of Mandrel Effect in Logging-While Drilling Propagation Tool," Well Logging Technical Report No. 32, pp. 102-120, 2011.
- [19] N. Yuan, R. Liu and X. Nie, "Electromagnetic Field of Arbitrarily Oriented Coil Antennas in Complex Underground Environment," Progress in Electromagnetics Research B, vol. 44, 261-282, 2012.
- [20] X. Lu, D. L. Alumbaugh and C. J. Weiss, "The Electric Fields and Currents Produced by Induction Logging Instruments in Anisotropic Media," Geophysics, vol. 67, no. 2, 478-483, 2002.
- [21] D. Omeragic, L. Sun, V. Polyakov, Y. Chen, X. Cao, T. Habashy, T. vok, J. Rasmus and J. Denichou, "Characterizing Teardrop Invasion in Horizontal Wells in the Presence of Boundaries using LWD Directional Resistivity Measurements," 54th

Annual Society of Petrophysicists and Well Log Analysts (SPWLA) Symposium,
June 22-26, 2013.